Available online at www.sciencedirect.com
SCIENCE DIRECT®
Journal of Sound and Vibration 277 (2004) 239–275
JOURNAL OF SOUND AND VIBRATION
www.elsevier.com/locate/jsvi

Waves in stratified anisotropic poroelastic media: a transfer matrix approach

Anil K. Vashishth, Poonam Khurana*

Department of Mathematics, Kurukshetra University, Kurukshetra 136119, India

Received 24 February 2003; accepted 29 August 2003

Abstract

The problem of propagation of waves in multilayered anisotropic poroelastic medium is studied using the technique of transfer matrix. The model consists of a stack of anisotropic poroelastic solid layers overlying an anisotropic elastic solid layered half-space. The whole layered medium is lying under fluid half-space. The transfer matrices for anisotropic poroelastic layer and anisotropic elastic solid layer are derived. Using these matrices, reflection and transmission coefficients for the waves propagating in considered multilayered model are evaluated. The interface between the two stacks is considered to be imperfect and modified boundary conditions are applied thereat. Numerical computations are done for a particular model. The effects of porosity, anisotropy of the layers, thickness of the layers and imperfect bonding are studied on the wave propagation through the considered model. The results indicate that anisotropy of half-space is a very dominant property influencing the reflection–refraction phenomenon. Also, it is noticed that the imperfection of interface is accompanied by the dissipation of energy and the interface acts as an absorbing boundary.

1. Introduction

The concepts of fluid-saturated porous media have gained much attention in past years. The theory of poroelasticity has been proposed as a model for sediments to account for the acoustic and other properties which are not described by the fluid and the elastic theory alone. Biot [1,2] initiated the theory for elastic wave propagation in porous saturated materials which is very much general in nature and is formulated in such a way that quite general forms of solid and fluid may be incorporated, so representing a potentially powerful tool for studying the behavior of many

*Corresponding author.
E-mail address: poonam_khurana@yahoo.com (P. Khurana).

0022-460X/$ - see front matter © 2003 Elsevier Ltd. All rights reserved.
doi:10.1016/j.jsv.2003.08.024

different kinds of porous media. The theory takes into account the motion of the fluid and interconnected voids of a porous material and predicts the existence of three types of body waves, two dilatational and one shear. Practically, the saturated porous materials are anisotropic due to bedding, compaction and presence of micro-cracks. For instance, shales are naturally bedded and possess intrinsic anisotropy at the microscopic level. Similarly, compaction and presence of micro-cracks and fractures make the skeleton of a porous rock anisotropic.

Wave propagation in layered media has been a field of interest to many researchers due to its applications in different areas. The fundamental work on waves in layered media is reported in the classical text by Brekhovskikh [3]. Kennet [4] presented a detailed and systematic work on seismic wave propagation in stratified media. The ultrasonic of layered anisotropic media is very important due to applications in surface acoustic wave devices and composites [5–7]. In most ultrasonic applications, the transfer matrix method is utilized. The transfer matrix method in standard form was developed for general anisotropy in Refs. [7–9]. Soldatos and Ye [10] studied wave propagation in anisotropic laminated hollow cylinders of infinite extent.

Layered porous sequences have also attracted much attention because of their distinctive properties which are the topic of modern research. The applications of studies of layered fluid-saturated porous media cover a variety of fields, from physics to geophysics, engineering, soil-mechanics, underwater acoustics and non destructive evaluation. Wave propagation through layered porous media is analyzed by one or other method for many applications [11–17]. Reflection and transmission of seismic waves at the boundary of porous media are integral part of seismic studies of the earth's interior. The phenomenon in such a layered medium gives interesting data about mechanical and damping properties of the elementary layers and about effective media. The details of the behavior of solid can be easily extracted from the reflected wave field in the fluid and this study of influence of fluid loading on the interaction of elastic waves with elastic solids finds applications in the fields of geophysics, engineering, underwater explosions and sonar systems.

However, most of the work has been performed by taking into account either one or two of the physical properties of media at a time. The work presented, in this paper, is an effort to study the combined effects of different physical properties of media, e.g., layering, anisotropy, porosity, wave attenuation, imperfect boundaries, etc. on the propagation of waves. A multilayered model consisting layered stacks A and B of anisotropic poroelastic solid and anisotropic elastic solid, respectively, overlying an anisotropic elastic solid half-space is studied. First we summarize the Biot's theory of fluid-saturated poroelastic materials. The transfer matrices for anisotropic poroelastic layer and anisotropic elastic solid layer are obtained. Employing the technique of transfer matrices, the global matrices for the two stacks are determined. Imperfect bonding between the two stacks and the modified boundary conditions are discussed thereat. The analytical expressions of reflection and transmission coefficients in terms of the global matrix elements are then obtained. Finally, the numerical computations are done by limiting the total number of layers. The effects of variation in different properties of media are discussed in detail.

2. Biot theory for transversely isotropic porous solid and solutions of basic equations

According to Biot's theory [1,2], homogeneous porous solid matrix and its saturating fluid are treated in the manner of two interpenetrating elastic continua. Losses arise due to the viscous

motion of the fluid with relative to the solid matrix and due to viscoelasticity of frame. The equations of motion in a fluid-saturated porous medium are given by

$$\tau_{i1,1} + \tau_{i2,2} + \tau_{i3,3} = \rho\ddot{u}_i + \rho_f \ddot{W}_i \quad (i,j = 1,2,3),$$
$$-(p_f)_{,i} = \rho_f \ddot{u}_i + \frac{\hat{c}_i \rho_f}{\beta} \ddot{W}_i + F\hat{b}_i \dot{W}_i, \tag{1}$$

where β is the porosity, τ_{ij} are the total stress components acting on both the solid and fluid phases, measured per unit area of the porous material, p_f is the pore fluid pressure measured per unit area of the fluid, ρ_f is the mass density of the fluid, ρ is the bulk density of the porous material, u_i and U_i are the components of the average displacements of the solid and fluid phases respectively, $\dot{W}_i = \beta(\dot{U}_i - \dot{u}_i)$ are the components of fluid-discharge velocity denoting the flow of the fluid relative to the solid.

The dot (.) denotes the differentiation with respect to time t and comma before an index denotes the partial space derivative. The viscodynamic operator $F(\kappa)$ represents the friction between the solid and fluid phases. The forms of viscodynamic operator and the coefficient $\hat{b}_i$ were obtained by Biot for isotropic porous materials assuming the pores to be either circular or flat.

For circular pores

$$\hat{b}_i = \frac{\xi}{k_i}, \tag{2}$$

where ξ and k_i are the viscosity and permeability of the pore fluid, respectively.

For cylindrical pores, the permeability is given by

$$k_i = \left(\frac{8}{\bar{a}^2}\right)\delta_i, \tag{3}$$

where $\bar{a}$ is the pore size and δ_i is the shape factor and its value is one for circular cylindrical pores. The function $F(\kappa)$ and κ are defined as

$$F(\kappa) = \frac{\kappa T(\kappa)}{4\{1 - 2T(\kappa)/(\mathrm{i}\kappa)\}}, \quad T(\kappa) = \frac{ber'(\kappa) + \mathrm{i}\, bei'(\kappa)}{ber(\kappa) + \mathrm{i}\, bei(\kappa)}, \quad \kappa = \bar{a}\left(\frac{\omega\rho_f}{\xi}\right)^{1/2}, \tag{4}$$

where $ber(\kappa)$ and $bei(\kappa)$ are the real and imaginary parts of the Kelvin's function and primes denote their derivatives. ω is the angular frequency.

The $\hat{c}_i$ in Eqs. (1) are experimentally determined parameters that account for the fact that not all of the fluid moves in the direction of macroscopic pressure gradient because of the shape and orientation of the interstitial cavities. In the case of straight pores, these constants are unity.

The constitutive equations for a transversely isotropic porous solid (TIPS) medium [18], relating stresses to strains, are

$$\tau_{xx} = 2B_1 e_{xx} + B_2(e_{xx} + e_{yy}) + B_3 e_{zz} + B_6\zeta,$$
$$\tau_{yy} = 2B_1 e_{yy} + B_2(e_{xx} + e_{yy}) + B_3 e_{zz} + B_6\zeta,$$

$$\begin{aligned}
\tau_{zz} &= B_4 e_{zz} + B_3(e_{xx} + e_{yy}) + B_7\zeta,\\
\tau_{yz} &= 2B_5 e_{yz},\\
\tau_{zx} &= 2B_5 e_{zx},\\
\tau_{yz} &= 2B_1 e_{xy},\\
p_f &= B_6(e_{xx} + e_{yy}) + B_7 e_{zz} + B_8\zeta,
\end{aligned} \tag{5}$$

where

$$e_{ij} = \frac{1}{2}\left(\frac{\partial u_i}{\partial x_j} + \frac{\partial u_j}{\partial x_i}\right) \tag{6}$$

is the strain tensor of the solid phase of the porous solid, and $\zeta = div[\beta(\mathbf{u} - \mathbf{U})]$ is the increment of fluid content per unit volume of the porous material, i.e., the amount of fluid which has flowed in and out of the given element attached to the solid frame. The coefficients $B_1, B_2, \ldots, B_8$ appearing in Eqs. (5) are elastic coefficients for a TIPS. These eight elastic coefficients are chosen in order to constitute a symmetric matrix for transverse isotropic porous solid having z-axis as its axis of vertical symmetry. These are evaluated by the method developed by Hashin and Rosen [19] and by Christensen [20] for evaluating the material coefficients of composite materials. These are given by

$$\begin{aligned}
B_1 &= \mu_{12},\\
B_2 &= K_{12} - \mu_{12},\\
B_3 &= 2\nu_{31}K_{12},\\
B_4 &= E_{33} + 4\nu_{31}^2 K_{12},\\
B_5 &= \mu_{13},
\end{aligned}$$

$$\begin{aligned}
B_6 &= -\frac{K_f(K_s + 4\mu_s/3)}{K_f + \mu_s + \beta(K_s + \mu_s/3 - K_f)},\\
B_7 &= -K_f\left[1 + (1-\beta)\frac{2\nu_s(K_s + \mu_s/3) - K_f}{K_f + \mu_s + \beta(K_s + \mu_s/3 - K_f)}\right],\\
B_8 &= \frac{K_f[(K_s + \mu_s/3)\beta + \mu_s]}{K_f + \mu_s + \beta(K_s + \mu_s/3 - K_f)},
\end{aligned}$$

where

$$\begin{aligned}
E_{33} &= (1-\beta)E_s + \frac{4\beta(1-\beta)(1/2 - \nu_s)^2}{(1-\beta)/K_f + \beta/(K_s + \mu_s/3) + 1/\mu_s},\\
\nu_{31} &= (1-\beta)\nu_s + \beta/2 + \frac{\beta(1-\beta)(1/2 - \nu_s)[1/(K_s + \mu_s/3) - 1/K_f]}{(1-\beta)/K_f + \beta/(K_s + \mu_s/3) + 1/\mu_s},\\
K_{12} &= K_s + \frac{\mu_s}{3} + \frac{\beta}{1/(K_f - K_s - \mu_s/3) + (1-\beta)/(K_s + 4\mu_s/3)},\\
\mu_{13} &= \frac{(1+\beta)}{(1-\beta)}\mu_s, \quad E_s = 2\mu_s(1 + \nu_s).
\end{aligned}$$

The coefficient μ_{12} is determined from the equation

$$A\left(\frac{\mu_{12}}{\mu_s}\right)^2 + 2B\left(\frac{\mu_{12}}{\mu_s}\right) + C = 0,$$

where

$$\begin{aligned} A &= -3\beta(1-\beta)^2 - (\eta_s + \beta^3)(1+\beta\eta_s),\\ B &= 3\beta(1-\beta)^2 + (1-\beta)(\eta_s - 1 + 2\beta^3)/2 - \beta/2(\eta_s+1)(1-\beta^3),\\ C &= -3\beta(1-\beta)^2 + (1-\beta)(1-\beta^3),\\ \eta_s &= 3 - 4\nu_s. \end{aligned} \tag{7}$$

In the above relations, K_s, μ_s, E_s and ν_s are the bulk modulus, shear modulus, Young's modulus and the Poisson ratio of the solid frame matrix, respectively. K_f is bulk modulus of the interstitial pore fluid.

Consider two-dimensional wave motion in xz-plane. The plane harmonic wave solutions of Eqs. (1) can be written in the form

$$\begin{aligned} u_x &= a_1 \exp\left(\mathrm{i}\omega\left(t - \frac{x}{c} - qz\right)\right),\\ u_z &= a_3 \exp\left(\mathrm{i}\omega\left(t - \frac{x}{c} - qz\right)\right),\\ W_x &= b_1 \exp\left(\mathrm{i}\omega\left(t - \frac{x}{c} - qz\right)\right),\\ W_z &= b_3 \exp\left(\mathrm{i}\omega\left(t - \frac{x}{c} - qz\right)\right), \end{aligned} \tag{8}$$

where a_1, a_3, b_1 and b_3 are the wave amplitudes, c is the apparent phase velocity. Substituting these solutions in Eqs. (1)–(6), we obtain a system of four equations in a_1, a_3, b_1 and b_3, the non-trivial solution of this system exists when

$$\begin{vmatrix} \{\rho - B_5q^2 - (2B_1+B_2)/c^2\} & -(B_3+B_5)(\frac{q}{c}) & (B_6/c^2+\rho_f) & B_6(\frac{q}{c}) \\ -(B_3+B_5)(\frac{q}{c}) & \{\rho - B_4q^2 - B_5/c^2\} & B_7(\frac{q}{c}) & (\rho_f + B_7q^2) \\ (B_6/c^2+\rho_f) & B_7(\frac{q}{c}) & \{-B_8/c^2 + \frac{\hat{c}_1\rho_f}{\beta} - \mathrm{i}F\hat{b}_1/\omega\} & -B_8(\frac{q}{c}) \\ B_6(\frac{q}{c}) & (\rho_f + B_7q^2) & -B_8(\frac{q}{c}) & \{-B_8q^2 + \frac{\hat{c}_3\rho_f}{\beta} - \mathrm{i}F\hat{b}_3/\omega\} \end{vmatrix} = 0. \tag{9}$$

Expansion of the determinant gives a cubic in q^2 which can be written as

$$T_0q^6 + T_1q^4 + T_2q^2 + T_3 = 0, \tag{10}$$

where

$$\begin{aligned} T_0 &= C_{11}B_5(B_7^2 - B_4B_8),\\ T_1 &= T_{11} + T_{12}/c^2,\\ T_2 &= T_{21} + T_{22}/c^2 + T_{23}/c^4,\\ T_3 &= T_{31} + T_{32}/c^2 + T_{33}/c^4 + T_{34}/c^6, \end{aligned}$$

$$
\begin{aligned}
T_{11} &= C_{11}(B_4B_8 - B_7^2)\rho + C_{11}\rho B_5B_8 + 2C_{11}\rho_f B_5B_7 + C_{11}C_{33}B_4B_5 - \rho_f^2(B_4B_8 - B_7^2),\\
T_{12} &= C_{11}(2B_1 + B_2)(B_7^2 - B_4B_8) - C_{33}B_4B_5B_8 + C_{33}B_5B_7^2 + C_{11}(B_3^2B_8 + 2B_3B_5B_8)\\
&\quad - C_{11}B_6(2B_3B_7 + 2B_5B_7 - B_4B_6),\\
T_{21} &= -C_{11}\rho^2B_8 - 2C_{11}\rho\rho_f B_7 - C_{33}C_{11}\rho(B_4 + B_5) + C_{11}\rho_f^2B_5 + C_{33}\rho_f^2B_4 + \rho\rho_f^2B_8 + 2B_7\rho_f^3,\\
T_{22} &= \rho(C_{11}B_5B_8 + C_{33}B_4B_8) + \rho C_{11}(2B_1 + B_2)B_8 + 2C_{11}B_7\rho_f(2B_1 + B_2) - C_{33}\rho B_7^2\\
&\quad + C_{11}C_{33}B_4(2B_1 + B_2) + C_{33}\rho B_5B_8 - 4\rho_f^2B_5B_8 - 2\rho_f(B_3 + B_5)(C_{11}B_6 + C_{33}B_7)\\
&\quad - 2\rho_f^2B_3B_8 - C_{11}C_{33}(B_3^2 - 2B_3B_5) + 2C_{33}\rho_f B_4B_8 + 2\rho_f^2B_6B_7 - C_{11}\rho B_6^2,\\
T_{23} &= C_{33}B_7^2(2B_1 + B_2) - (C_{11}B_5 + C_{33}B_4)\{(2B_1 + B_2)B_8 - B_6^2\} + C_{33}(B_3 + B_5)(B_3B_8 - 2B_6B_7),\\
T_{31} &= \rho^2C_{11}C_{33} - \rho\rho_f^2(C_{11} + C_{33}) + \rho_f^4,\\
T_{32} &= \rho C_{33}\{C_{11}(B_5 + 2B_1 + B_2) - \rho B_8 - 2\rho_f B_6\} + \rho_f^2\{\rho B_8 + 2\rho_f B_6 + C_{11}(2B_1 + B_2) + C_{33}B_5\},\\
T_{33} &= \rho C_{33}B_8(B_5 + 2B_1 + B_2) + C_{33}C_{11}B_5(2B_1 + B_2) + \rho_f^2\{B_6^2 - B_8(2B_1 + B_2)\}\\
&\quad + C_{33}B_6(2\rho_f B_5 - \rho B_8),\\
T_{34} &= C_{33}B_5\{B_6^2 - B_8(2B_1 + B_2)\},\\
C_{11} &= \frac{\hat{c}_1\rho_f}{\beta} - \mathrm{i}\frac{F\hat{b}_1}{\omega}, \quad C_{33} = \frac{\hat{c}_3\rho_f}{\beta} - \mathrm{i}\frac{F\hat{b}_3}{\omega}.
\end{aligned}
\tag{11}
$$

The roots of Eq. (10) are, in general, complex. We denote these roots by $q(n)$, $n = 1, 2, \ldots, 6$. Three roots with positive real parts correspond to the waves traveling in the positive z direction (downgoing waves) and the other three roots with negative real parts correspond to the waves traveling in the negative z direction (upgoing waves). We order the six roots $q(n)$, $n = 1, 2, \ldots, 6$ such that $q(1)$, $q(2)$, $q(3)$ correspond to the three upgoing waves, namely quasi-P_f, quasi-P_s and quasi-SV waves respectively; and $q(6)$, $q(5)$ and $q(4)$ correspond to the downgoing quasi-P_f, quasi-P_s and quasi-SV waves respectively.

Thus, we write

$$q(1) = -q(6), \quad q(2) = -q(5), \quad q(3) = -q(4). \tag{12}$$

Eq. (10), a cubic in q^2, has three equal roots if

$$\hat{Q} = \frac{T_1^2 - 3T_0T_2}{9T_0^2} = 0,$$

and two equal roots, if

$$\hat{R} = \frac{2T_1^3 - 9T_0T_1T_2 + 27T_0^2T_3}{54T_0^3} = 0.$$

In general, the expressions of $\hat{Q}$ and $\hat{R}$ are non-zero implying that all the roots of Eq. (10) are distinct. It is unlikely that the roots are repeated. These three roots correspond to quasi-P_f, -P_s and -SV waves in transversely isotropic poroelastic medium. In case of isotropic poroelastic medium, they reduce to the ones which are known to be distinct and correspond to P_f, P_s and SV waves respectively.

The wave amplitudes a_1, a_3, b_1 and b_3 are obtained. These are given by

$$a_1(n) = \frac{X_1(n)}{X(n)}, \quad a_3(n) = \frac{X_2(n)}{X(n)}, \quad b_1(n) = \frac{X_3(n)}{X(n)}, \quad b_3(n) = \frac{X_4(n)}{X(n)}, \tag{13}$$

where

$$\begin{aligned} X_1(n) = {} & q^4(n)C_{11}(B_4B_8 - B_7^2) \\ & + q^2(n)\{B_8(B_5C_{11} + B_4C_{33})/c^2 - 2C_{11}\rho_f B_7 - \rho C_{11}B_8 + C_{33}(-C_{11}B_4 - B_7^2/c^2)\} \\ & + \left\{ C_{33}\frac{B_8}{c^2}(B_5/c^2 - \rho) - C_{11}C_{33}(B_5/c^2 - \rho) + \rho_f^2(B_8/c^2 - C_{11}) \right\}, \end{aligned}$$

$$\begin{aligned} X_2(n) = {} & \frac{q^3(n)}{c} C_{11}(B_6B_7 - B_3B_8 - B_5B_8) \\ & + \frac{q(n)}{c}[\{B_7(\rho_f + B_6/c^2) - B_8(B_3 + B_5)/c^2\}C_{33}] \\ & + \frac{q(n)}{c}[C_{11}\rho_f B_6 + \rho_f^2 B_8 + C_{33}C_{11}(B_3 + B_5)], \end{aligned}$$

$$\begin{aligned} X_3(n) = {} & q^4(n)\rho_f(B_7^2 - B_4B_8) + q^2(n)\{B_4C_{33}(\rho_f + B_6/c^2) - (C_{33}B_7 + \rho_f B_8)(B_3 + B_5)/c^2\} \\ & + q^2(n)\{\rho_f B_8(\rho - B_5/c^2) + \rho_f B_7(\rho_f + B_6/c^2) + B_7\rho_f^2\} \\ & + (\rho_f + B_6/c^2)(\rho_f^2 - C_{33}(\rho - B_5/c^2)), \end{aligned}$$

$$\begin{aligned} X_4(n) = {} & \frac{q^3(n)}{c}\{C_{11}(B_4B_6 - B_3B_7 - B_5B_7) + (B_4B_8 - B_7^2)\rho_f\} + \frac{q(n)}{c} \\ & \times \{-C_{11}\rho_f(B_3 + B_5) + C_{11}(B_5/c^2 - \rho)B_6 + \rho_f B_8(B_3 + 2B_5)/c^2 \\ & - \rho\rho_f B_8 - \rho_f B_7(\rho_f + B_6/c^2)\}, \end{aligned}$$

and

$$X(n) = \sqrt{(X_1(n))^2 + (X_2(n))^2 + (X_3(n))^2 + (X_4(n))^2}.$$

The displacement components associated with the quasi body waves in a transversely isotropic porous solid layer can, then, be written in the form

$$u_x = \sum_{n=1}^{6} f(n)a_1(n)\exp\left(\mathrm{i}\omega\left(t - \frac{x}{c} - q(n)z\right)\right),$$

$$u_z = \sum_{n=1}^{6} f(n)a_3(n)\exp\left(\mathrm{i}\omega\left(t - \frac{x}{c} - q(n)z\right)\right),$$

$$W_x = \sum_{n=1}^{6} f(n) b_1(n) \exp\left(\mathrm{i}\omega\left(t - \frac{x}{c} - q(n)z\right)\right),$$

$$W_z = \sum_{n=1}^{6} f(n) b_3(n) \exp\left(\mathrm{i}\omega\left(t - \frac{x}{c} - q(n)z\right)\right), \tag{14}$$

where $f(n)$ are relative amplitudes of transmitted quasi-P_f, quasi-P_s and quasi-SV waves to that of incident wave.

3. Formulation of problem

We consider a stack A of transversely isotropic poroelastic solid (TIPS) layers overlying another stack B of transversely isotropic elastic solid (TIES) layers. Let medium A has n layers and medium B has m layers. Thus, we have in total $(n+m)$ layers and the whole $(n+m)$-layered medium is underlying a fluid half-space (FHS) and overlying a transversely isotropic elastic solid (TIES) half-space. The geometry of medium is shown in Fig. 1a. Consider the case of incident P wave in the FHS which makes an angle θ with the normal to the boundary. Incidence of P wave at the interface between FHS and the first TIPS layer results into one reflected P wave and three transmitted (quasi-P_f, quasi-P_s and quasi-SV) waves in the porous layer. These waves, when strike the next boundary, give rise to three reflected waves and three transmitted waves and this process goes on. Similarly, four quasi waves (two upgoing and two downgoing), propagate in TIES layer. Finally, two waves (quasi-P and -SV) are transmitted into the TIES half-space, as shown in Fig. 1a.

Consider the pth layer of thickness $d^{(p)}$ bounded between the pth and $(p+1)$st interfaces. The superscript 'p' is used to denote the quantities of the pth TIPS layer. The displacements associated with the upgoing and downgoing body waves in pth TIPS layer are written as

$$u_x^{(p)} = \sum_{n=1}^{6} f^{(p)}(n) a_1^{(p)}(n) \exp\left(\mathrm{i}\omega\left(t - \frac{x}{c} - q^{(p)}(n)z\right)\right),$$

$$u_z^{(p)} = \sum_{n=1}^{6} f^{(p)}(n) a_3^{(p)}(n) \exp\left(\mathrm{i}\omega\left(t - \frac{x}{c} - q^{(p)}(n)z\right)\right),$$

$$W_x^{(p)} = \sum_{n=1}^{6} f^{(p)}(n) b_1^{(p)}(n) \exp\left(\mathrm{i}\omega\left(t - \frac{x}{c} - q^{(p)}(n)z\right)\right),$$

$$W_z^{(p)} = \sum_{n=1}^{6} f^{(p)}(n) b_3^{(p)}(n) \exp\left(\mathrm{i}\omega\left(t - \frac{x}{c} - q^{(p)}(n)z\right)\right). \tag{15}$$

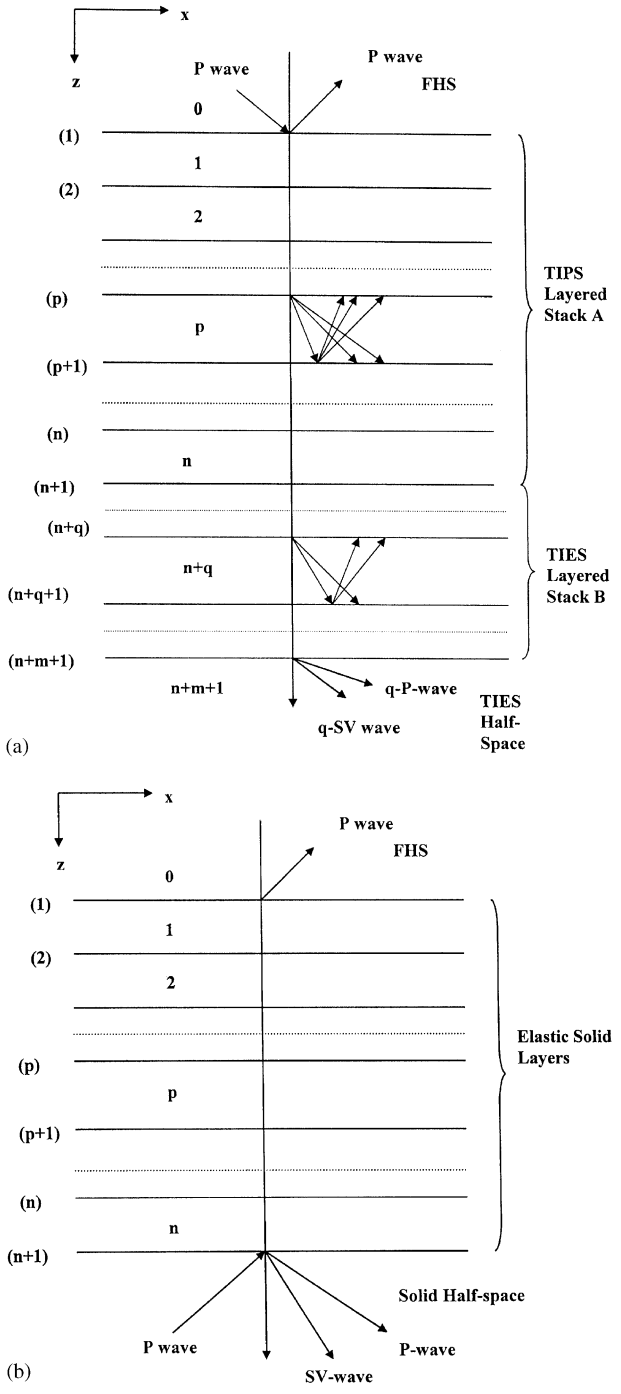

Fig. 1. (a) Geometry of the medium; (b) core–mantle boundary model.

4. Transfer matrix for anisotropic poroelastic layered stack

Let the displacement–stress field in pth TIPS layer be described by the column vector given by $\mathbf{V}^{(p)}(z) = [u_x^{(p)} \;\; u_z^{(p)} \;\; W_z^{(p)} \;\; \tau_{zz}^{(p)} \;\; \tau_{zx}^{(p)} \;\; p_f^{(p)}]^{\mathrm{T}}$. This can be expressed as the function of amplitudes by the relation

$$\mathbf{V}^{(p)}(z) = [\Gamma^{(p)}(z)]\mathbf{A}^{(p)}, \tag{16}$$

where $\mathbf{A}^{(p)} = [(f^{(p)}(1) + f^{(p)}(6)) \;\; (f^{(p)}(1) - f^{(p)}(6)) \;\; (f^{(p)}(2) + f^{(p)}(5)) \;\; (f^{(p)}(2) - f^{(p)}(5)) \;\; (f^{(p)}(3) + f^{(p)}(4)) \;\; (f^{(p)}(3) - f^{(p)}(4))]^{\mathrm{T}}$ is the amplitude vector, $[\Gamma^{(p)}(z)]$ is the matrix of order 6 and its elements are given in Appendix A.

The matrix relation (16) enables us to express the displacement–stress field at the upper surface of the pth layer as the function of that at the lower surface. Eliminating the common amplitudes from the equations

$$\mathbf{V}_p = [\Gamma_p]\mathbf{A}^{(p)} \quad \text{and} \quad \mathbf{V}_{p+1} = [\Gamma_{p+1}]\mathbf{A}^{(p)} \tag{17}$$

we get

$$\mathbf{V}_p = [\Gamma_p][\Gamma_{p+1}]^{-1}\mathbf{V}_{p+1}, \tag{18}$$

where $\mathbf{V}_p$, $[\Gamma_p]$ and $\mathbf{V}_{p+1}$, $[\Gamma_{p+1}]$ are the values of $\mathbf{V}^{(p)}(z)$ and $[\Gamma^{(p)}(z)]$ at pth and $(p+1)$st interface, respectively, $[\Gamma_{p+1}]^{-1}$ is obtained by evaluating the $[\Gamma^{(p)}(z)]^{-1}$ at $(p+1)$st interface.

Eq. (18) can be written as

$$\mathbf{V}_p = [T^{(p)}]\mathbf{V}_{p+1}, \tag{19}$$

where $[T^{(p)}] = [\Gamma_p][\Gamma_{p+1}]^{-1}$ is the local transfer matrix for the pth layer relating its displacement–stress field vector on the two faces of the layer.

By successive repetition of the above process for each layer ($p = 1, 2, \ldots, n$) and by invoking the continuity conditions of displacements and stresses at the common surfaces in the layered anisotropic poroelastic medium, we could relate the displacements and stresses at the upper surface of the stack to those at its lower surface through a matrix relation. The local matrix for each layer is of the same type as obtained for the pth layer.

Thus, if we denote

$$[T] = \prod_{r=1}^{n} [T^{(r)}] \tag{20}$$

then, we can write

$$\mathbf{V}_1 = [T]\mathbf{V}_{n+1}, \tag{21}$$

where $\mathbf{V}_1 = \mathbf{V}^{(1)}(z)$ and $\mathbf{V}_{n+1} = \mathbf{V}^{(n)}(z)$ are the displacement–stress vectors evaluated at the first interface ($z = 0$) and at the $(n+1)$st interface ($z = d^{(1)} + d^{(2)} + \cdots + d^{(n)}$).

5. Basic equations for transversely isotropic elastic solid

Following Love [21], the equations of motion for transversely isotropic solid are

$$\tau^s_{ij,j} = \rho^s u^s_i \quad (i,j = 1,2,3), \tag{22}$$

where $\tau^s_{ij,j}$, u^s_i, ρ^s are the stresses, displacements and density in the transversely isotropic solid respectively. Considering the motion in the xz-plane, the constitutive equations are written as

$$\begin{aligned}
\tau^s_{xx} &= A^s e^s_{xx} + F^s e^s_{zz} = A^s \frac{\partial u^s}{\partial x} + F^s \frac{\partial w^s}{\partial z},\\
\tau^s_{xz} &= 2L^s e^s_{xz} = L^s \left(\frac{\partial u^s}{\partial z} + \frac{\partial w^s}{\partial x} \right),\\
\tau^s_{zz} &= C^s e^s_{zz} + F^s e^s_{xx} = C^s \frac{\partial w^s}{\partial z} + F^s \frac{\partial u^s}{\partial x},
\end{aligned} \tag{23}$$

where A^s, L^s, F^s and C^s are elastic constants and u^s, w^s are the displacement components along x- and z-axis, respectively.

We seek the solution of Eqs. (22) of the form

$$\begin{aligned}
u^s &= P^s \exp \mathrm{i}k(ct - x - sz),\\
w^s &= Q^s \exp \mathrm{i}k(ct - x - sz).
\end{aligned} \tag{24}$$

Substituting this solution into Eqs. (23), we obtain a system of two equations in P^s and Q^s, non-trivial solution of which exists if

$$(s)^4 L^s C^s + (s)^2(-L^s N^s - R^s C^s - (J^s)^2) + R^s N^s = 0, \tag{25}$$

where $J^s = (F^s + L^s)$, $R^s = \rho^s c^2 - A^s$, $N^s = \rho^s c^2 - L^s$.

This equation being quadratic in $(s)^2$, has solutions as

$$(s_j)^2 = \frac{M^s + (-1)^j \sqrt{(M^s)^2 - 4L^s C^s R^s N^s}}{2L^s C^s} \quad (j = 1,2), \tag{26}$$

where $M^s = L^s N^s + R^s C^s + (J^s)^2$.

The ratio of the displacement components u^s_j, w^s_j corresponding to $s = s_j$, is given by

$$\frac{w^s_j}{u^s_j} = \frac{Q^s_j}{P^s_j} = -\frac{L^s (s_j)^2 - R^s}{s_j J^s} = \boldsymbol{m}_j \text{ (say)} \quad (j = 1,2). \tag{27}$$

Thus, the solution of Eqs. (22) can be written as

$$u^s = [\mathrm{e}^{\pm \mathrm{i}ks_1 z} + \mathrm{e}^{\pm \mathrm{i}ks_2 z}] \exp \mathrm{i}k(ct - x)$$

or

$$u^s = [P^s_1 \mathrm{e}^{-\mathrm{i}ks_1 z} + P^s_2 \mathrm{e}^{-\mathrm{i}ks_2 z} + P^s_3 \mathrm{e}^{\mathrm{i}ks_1 z} + P^s_4 \mathrm{e}^{\mathrm{i}ks_2 z}] \exp \mathrm{i}k(ct - x), \tag{28}$$

where P^s_1, P^s_2, P^s_3, P^s_4 are arbitrary constants.

The corresponding expression of w^s can now be written as

$$w^s = [m_1(P_1^s e^{-ik s_1 z} - P_3^s e^{ik s_1 z}) + m_2(P_2^s e^{-ik s_2 z} - P_4^s e^{ik s_2 z})] \exp ik(ct - x). \tag{29}$$

The stress components can be determined by substituting the expressions of displacements from Eqs. (28) and (29) into Eqs. (23).

6. Transfer matrix for anisotropic elastic layered stack

Consider the qth layer of TIES bounded between the $(n+q)$th and $(n+q+1)$st interfaces. The superscript 'q' is used to denote the quantities of the qth TIES layer. The displacements associated with the upgoing and downgoing body waves in qth layer are

$$u^{s(q)} = [P_1^{s(q)} e^{-ik s_1^{(q)} z} + P_2^{s(q)} e^{-ik s_2^{(q)} z} + P_3^{s(q)} e^{ik s_1^{(q)} z} + P_4^{s(q)} e^{ik s_2^{(q)} z}] \exp ik(ct - x),$$

$$w^{s(q)} = [m_1^{(q)}(P_1^{s(q)} e^{-ik s_1^{(q)} z} - P_3^{s(q)} e^{ik s_1^{(q) z}}) + m_2^{(q)}(P_2^{s(q)} e^{-ik s_2^{(q)} z} - P_4^{s(q)} e^{ik s_2^{(q)} z})] \exp ik(ct - x).$$

Defining the field vector in qth layer by $\mathbf{V}^{s(q)}(z) = [u^{s(q)} \;\; w^{s(q)} \;\; \tau_{zz}^{s(q)} \;\; \tau_{zx}^{s(q)}]$ and amplitude vector by $\mathbf{A}^{s(q)} = [(P_1^{s(q)} + P_3^{s(q)}) \;\; (P_1^{s(q)} - P_3^{s(q)}) \;\; (P_2^{s(q)} + P_4^{s(q)}) \;\; (P_2^{s(q)} - P_4^{s(q)})]$, we write the expressions of displacements and stresses in the matrix form as

$$\mathbf{V}^{s(q)}(z) = [\Gamma^{s(q)}(z)]\mathbf{A}^{s(q)}, \tag{30}$$

where $[\Gamma^{s(q)}(z)]$ is a 6×6 matrix obtained by the coefficients of elements of $\mathbf{A}^{s(q)}$ and its elements are given in Appendix B.

Eq. (30) holds for each layer q, $(= n+1, \ldots, n+m)$ of the stack B. The transfer matrix $[T^{s(q)}]$ is determined by the product of the matrix $[\Gamma^{s(q)}(z)]$ evaluated at the upper surface of the layer, i.e., at $(n+q)$th interface and $[\Gamma^{s(q)}(z)]^{-1}$ at the lower surface, i.e., at $(n+q+1)$th interface.

Applying the same procedure for each layer of the stack B of TIES layers and using the continuity conditions of the displacements and stresses at each interface of the layered anisotropic solid medium, the displacement–stress field vector at the uppermost surface of the stack B is related to its lowermost surface. Denoting the global matrix of the layered anisotropic medium by $[T^s]$, we write

$$[T^s] = \prod_{q=(n+1)}^{(n+m)} [T^{s(q)}]. \tag{31}$$

This results in

$$\mathbf{V}_{n+1} = [T^s]\mathbf{V}_{n+m+1}, \tag{32}$$

where $\mathbf{V}_{n+1}$ and $\mathbf{V}_{n+m+1}$ are the displacement–stress vectors at the upper and lower faces of the TIES stack B, respectively.

Expressing the displacement–stress field vector in TIES half-space as

$$\mathbf{V}^{(n+m+1)}(z) = [\varepsilon^{(n+m+1)}] \begin{bmatrix} P_1^{s(n+m+1)} \\ P_2^{s(n+m+1)} \end{bmatrix}, \tag{33}$$

where $[\varepsilon^{(n+m+1)}]$ is the 4×2 matrix obtained from the coefficients of amplitudes $P_1^{s(n+m+1)}$ and $P_2^{s(n+m+1)}$ of transmitted quasi-P and -SV waves in TIES half-space and is given in Appendix B.

From the continuity of displacements and stresses at $(n+m)$th interface, it follows that $\mathbf{V}^{(n+m+1)}(z) = \mathbf{V}^{(n+m)}(z)$ at the $(n+m)$th interface or

$$\mathbf{V}^{(n+m+1)} = \mathbf{V}_{n+m+1}. \tag{34}$$

This implies that

$$\mathbf{V}_{n+1} = [T^s][\varepsilon^{(n+m+1)}] \begin{bmatrix} P_1^{s(n+m+1)} \\ P_2^{s(n+m+1)} \end{bmatrix}. \tag{35}$$

The displacement potential in the FHS, satisfying the wave equation, is

$$\phi = (\mathrm{e}^{-\mathrm{i}kr_\alpha z} + R\mathrm{e}^{\mathrm{i}kr_\alpha z}) \exp\{\mathrm{i}k(ct - x)\}, \tag{36}$$

where $r_\alpha = \sqrt{c^2/\alpha^2 - 1}$, α being the P wave velocity in the fluid and R is the reflection coefficient.

The normal displacement u_z and the pressure p in the FHS are given by

$$u_z = \mathrm{i}kr_\alpha(R\mathrm{e}^{\mathrm{i}kr_\alpha z} - \mathrm{e}^{-\mathrm{i}kr_\alpha z}) \exp\{\mathrm{i}k(ct - x)\}, \tag{37}$$

$$p = -\lambda\nabla^2\phi = \rho\omega^2(\mathrm{e}^{-\mathrm{i}kr_\alpha z} + R\mathrm{e}^{\mathrm{i}kr_\alpha z}) \exp\{\mathrm{i}k(ct - x)\}. \tag{38}$$

7. Boundary conditions

The bonding between the stack A of TIPS layers and stack B of TIES layers is considered not to be perfect and does not ensure the continuity of tangential displacement. Following Vashishth et al. [22], the modified boundary conditions to be applied at such an interface, i.e., $(n+1)$st interface, are

$$u_z^{(n)} = u_z^{(n+1)}, \tag{39a}$$

$$W_z^{(n)} = 0, \tag{39b}$$

$$\tau_{zz}^{(n)} = \tau_{zz}^{(n+1)}, \tag{39c}$$

$$\tau_{zx}^{(n)} = \tau_{zx}^{(n+1)}, \tag{39d}$$

$$\tau_{zx}^{(n)} = \mathrm{i}\omega \frac{\mu^{(n+1)}}{\alpha_s^{(n+1)}} \frac{\psi}{(1-\psi)} (u_x^{(n)} - u_x^{(n+1)}), \tag{39e}$$

where quantities with superscript $(n+1)$ correspond to the $(n+1)$st TIES layer and those with the superscript (n) correspond to the nth TIPS layer.

The boundary conditions at interface $z = 0$ between the FHS and first TIPS layer are

$$u_z^{(1)} + W_z^{(1)} = u_z, \tag{40}$$

$$\tau_{zz}^{(1)} = -p, \tag{41}$$

$$p_f^{(1)} = p, \tag{42}$$

$$\tau_{zx}^{(1)} = 0, \tag{43}$$

where the quantities with superscript 1 correspond to the first TIPS layer.

The boundary conditions (39) along with Eq. (43) provides us an interfacial matrix $[\eta]_{6\times4}$, relating the displacement–stress vectors of nth and $(n+1)$st layers. Thus, we can write

$$\mathbf{V}^{(n)}(z) = [\eta]\mathbf{V}^{(n+1)}(z) \text{ at } (n+1)\text{st interface}$$

which implies that

$$\mathbf{V}_{n+1} = [\eta][T^s][\varepsilon^{(n+m+1)}]\begin{bmatrix} P_1^{s(n+m+1)} \\ P_2^{s(n+m+1)} \end{bmatrix}. \tag{44}$$

Using Eq. (21), we obtain the condensed form expression for $\mathbf{V}_1$ as

$$\mathbf{V}_1 = [T][\eta][T^s][\varepsilon^{(n+m+1)}]\begin{bmatrix} P_1^{s(n+m+1)} \\ P_2^{s(n+m+1)} \end{bmatrix} \quad \text{or} \quad \mathbf{V}_1 = [C]\begin{bmatrix} P_1^{s(n+m+1)} \\ P_2^{s(n+m+1)} \end{bmatrix}, \tag{45}$$

where $[C] = [T][\eta][T^s][\varepsilon^{(n+m+1)}]$, a 6×2 matrix, is the global transfer matrix for the whole $(n+m+1)$-layered medium.

Utilizing Eqs. (37), (38) and (45) into the boundary conditions (40)–(42), we obtain

$$\begin{aligned} &(C_{21}+C_{31})P_1^{s(n+m+1)} + (C_{22}+C_{32})P_2^{s(n+m+1)} - \mathrm{i}kr_\alpha R = -\mathrm{i}kr_\alpha, \\ &C_{41}P_1^{s(n+m+1)} + C_{42}P_2^{s(n+m+1)} + \rho\omega^2 R = -\rho\omega^2, \\ &C_{61}P_1^{s(n+m+1)} + C_{62}P_2^{s(n+m+1)} - \rho\omega^2 R = \rho\omega^2. \end{aligned} \tag{46}$$

Solving the above equations, the analytical expressions of reflection coefficient (R), transmission coefficients of q-P wave and q-SV wave are obtained as

$$\begin{aligned} R &= \frac{\Delta_2 - Q_f\Delta_1}{\Delta_2 + Q_f\Delta_1}, \\ P_1^{s(n+m+1)} &= \frac{-2\rho\omega^2(C_{42}+C_{62})}{\Delta_2 + Q_f\Delta_1}, \quad P_2^{s(n+m+1)} = \frac{2\rho\omega^2(C_{41}+C_{61})}{\Delta_2 + Q_f\Delta_1}, \end{aligned} \tag{47}$$

where

$$\Delta_1 = \begin{vmatrix} (C_{21}+C_{31}) & (C_{22}+C_{32}) \\ (C_{41}+C_{61}) & (C_{42}+C_{62}) \end{vmatrix}, \quad \Delta_2 = \begin{vmatrix} C_{41} & C_{42} \\ C_{61} & C_{62} \end{vmatrix}, \quad Q_f = \frac{\rho\omega^2}{\mathrm{i}kr_\alpha}.$$

The expressions of the reflection and transmission coefficients yield, as a by-product, the characteristic equation for the propagation of surface waves in the considered model. On putting the denominator $\Delta_2 + Q_f\Delta_1 = 0$, we get the frequency equation for the propagation of generalized Rayleigh waves on the surface of a fluid-loaded layered anisotropic poroelastic medium bonded loosely to layered anisotropic elastic solid substrate. The frequency equation is given by

$$Q_f\{(C_{21}+C_{31})(C_{42}+C_{62}) - (C_{41}+C_{61})(C_{32}+C_{22})\} + (C_{41}C_{62} - C_{42}C_{61}) = 0. \tag{48}$$

In the absence of FHS, i.e., the case when $\rho = 0$, the frequency equation (48) reduces to $\Delta_2 = (C_{41}C_{62} - C_{42}C_{61}) = 0$.

This is the frequency equation of surface waves propagating on the free surface of anisotropic poroelastic layered medium bonded loosely to a layered anisotropic elastic solid substrate.

8. Application of transfer matrix to core–mantle boundary model

In order to verify the solutions obtained by the present approach in comparison with the other model and in order to broaden the application of the transfer function technique to various core phases, this study first derives a complete complex transfer matrix and then applies that to get reflection and transmission coefficients when a plane P wave is incident at the plane layered core–mantle boundary. The geometry of the model for core–mantle boundary is given in Fig. 1(b).

The displacement potential in the FHS can be considered as

$$\phi = T\mathrm{e}^{\mathrm{i}kr_\alpha z}\mathrm{e}^{\mathrm{i}k(ct-x)}, \tag{49}$$

where T is the transmission coefficient.

The displacement potentials in the mantle (EHS) are

$$\begin{aligned}\phi^{(n+1)} &= (\mathrm{e}^{\mathrm{i}kr_\alpha^{(n+1)}z} + R_1\mathrm{e}^{-\mathrm{i}kr_\alpha^{(n+1)}z})\mathrm{e}^{\mathrm{i}k(ct-x)},\\ \psi^{(n+1)} &= R_2\mathrm{e}^{-\mathrm{i}kr_\beta^{(n+1)}z}\mathrm{e}^{\mathrm{i}k(ct-x)}\end{aligned} \tag{50}$$

where

$$r_\alpha^{(n+1)} = \begin{cases} (c^2/\alpha_{n+1}^2 - 1)^{1/2}, & c > \alpha_{n+1},\\ -\mathrm{i}(1 - c^2/\alpha_{n+1}^2)^{1/2}, & c < \alpha_{n+1},\end{cases}$$

and

$$r_\beta^{(n+1)} = \begin{cases} (c^2/\beta_{n+1}^2 - 1)^{1/2}, & c > \beta_{n+1},\\ -\mathrm{i}(1 - c^2/\beta_{n+1}^2)^{1/2}, & c < \beta_{n+1},\end{cases} \tag{51}$$

where R_1 and R_2 are the reflection coefficients of P and SV waves in EHS.

The displacement–stress vector $\mathbf{V}^{(n+1)}$ is obtained as

$$\mathbf{V}^{(n+1)} = [\varepsilon^{(n+1)}]\begin{bmatrix}1\\ R_1\\ R_2\end{bmatrix}, \tag{52}$$

where

$$\begin{aligned}\varepsilon_{11} &= -\mathrm{i}k\mathrm{e}^{\mathrm{i}kr_\alpha^{(n+1)}z}, \quad \varepsilon_{12} = -\mathrm{i}k\mathrm{e}^{-\mathrm{i}kr_\alpha^{(n+1)}z}, \quad \varepsilon_{13} = -\mathrm{i}kr_\beta^{(n+1)}\mathrm{e}^{-\mathrm{i}kr_\beta^{(n+1)}z},\\ \varepsilon_{21} &= \mathrm{i}kr_\alpha^{(n+1)}\mathrm{e}^{\mathrm{i}kr_\alpha^{(n+1)}z}, \quad \varepsilon_{22} = -\mathrm{i}kr_\alpha^{(n+1)}\mathrm{e}^{-\mathrm{i}kr_\alpha^{(n+1)}z}, \quad \varepsilon_{23} = -\mathrm{i}k\mathrm{e}^{-\mathrm{i}kr_\beta^{(n+1)}z},\\ \varepsilon_{31} &= -k^2\{\lambda - (\lambda + 2\mu)(r_\alpha^{(n+1)})^2\}\mathrm{e}^{\mathrm{i}kr_\alpha^{(n+1)}z},\\ \varepsilon_{32} &= -k^2\{\lambda - (\lambda + 2\mu)(r_\alpha^{(n+1)})^2\}\mathrm{e}^{-\mathrm{i}kr_\alpha^{(n+1)}z},\end{aligned}$$

$$\varepsilon_{33} = -2\mu k^2 r_\beta^{(n+1)} e^{-ikr_\beta^{(n+1)} z},$$
$$\varepsilon_{41} = 2\mu k^2 r_\alpha^{(n+1)} e^{ikr_\alpha^{(n+1)} z}, \quad \varepsilon_{42} = -2\mu k^2 r_\alpha^{(n+1)} e^{-ikr_\alpha^{(n+1)} z},$$
$$\varepsilon_{43} = -\mu k^2 (1 + (r_\beta^{(n+1)})^2) e^{-ikr_\beta^{(n+1)} z}.$$

The displacement–stress vector $\mathbf{V}_1$ is given by

$$\mathbf{V}_1 = [T^s][\varepsilon^{(n+1)}] \begin{bmatrix} 1 \\ R_1 \\ R_2 \end{bmatrix} = [P] \begin{bmatrix} 1 \\ R_1 \\ R_2 \end{bmatrix}, \tag{53}$$

where

$$[T^s] = \prod_{q=1}^{n} [T^{s(q)}] \quad \text{and} \quad [P] = [p_{ij}] = [T^\delta][\varepsilon^{(n+1)}]. \tag{54}$$

The boundary conditions at interface (1) are

$$\text{(i) } u_z^{(1)} = u_z^{(0)}, \quad \text{(ii) } \tau_{zz}^{(1)} = \tau_{zz}^{(0)}, \quad \text{(iii) } \tau_{xz}^{(1)} = 0. \tag{55}$$

Substitution of Eqs. (49) and (53) in the boundary conditions (55) and simplification of resulting equations leads to the evaluation of reflection and transmission coefficients. These are

$$R_1 = (ikr_\alpha(p_{44}p_{51} - p_{41}p_{54}) + \rho\omega^2(p_{24}p_{51} - p_{21}p_{54}))/\Delta,$$
$$R_2 = (-ikr_\alpha(p_{42}p_{51} - p_{41}p_{52}) + \rho\omega^2(p_{21}p_{52} - p_{22}p_{51}))/\Delta,$$

and

$$T = (-p_{21}(p_{52}p_{44} - p_{42}p_{54}) + p_{51}(p_{22}p_{44} - p_{24}p_{42}) - p_{41}(p_{22}p_{54} - p_{24}p_{52}))/\Delta,$$

where

$$\Delta = -ikr_\alpha(p_{52}p_{44} - p_{54}p_{42}) + \rho\omega^2(p_{22}p_{54} - p_{24}p_{52}). \tag{56}$$

9. Numerical results and discussion

Numerical calculations of the study were done for a particular model. The model consists of two layers, one transversely isotropic poroelastic solid (TIPS) layer and other transversely isotropic elastic solid (TIES) layer. These two layers are underlying a fluid half-space and overlying a transversely isotropic elastic solid half-space. The values of material coefficients for TIPS are taken from Yammamato [23] and are given in Table 1.

Using Eqs. (7), the values of the elastic constants $B_1^{(1)}, \ldots, B_8^{(1)}$ can be derived from the material coefficients given in Table 1. When the layer is isotropic, then

$$B_3^{(1)} = B_2^{(1)}, \quad B_6^{(1)} = B_7^{(1)}, \quad B_5^{(1)} = B_1^{(1)} \quad \text{and} \quad B_4^{(1)} = B_2^{(1)} + 2B_1^{(1)}.$$

The values of the elastic constants and density for TIES layer, TIEHS and FHS are given in Table 2.

Table 1
Material coefficients of TIPS layer (in CGS units)

Water saturated sandstone
$K_s = (5.33 \times 10^{11}, 15.99 \times 10^9)$
$E_s = (5.332 \times 10^{11}, 10.64 \times 10^8)$
$K_f = 2.3 \times 10^{10}$
$\mu_s = (2.0 \times 10^{11}, 4.0 \times 10^9)$
$v_s = 0.33$
$\rho_f = 1.025$
$\beta = 0.30$
$\xi = 1.0 \times 10^{-4}$
$\rho_s = 2.65$
$\hat{c}_1 = \hat{c}_3 = 1.25$

For these values of elastic parameters, the reflection and transmission coefficients of the above stated numerical model were computed. The values of non-dimensional wave number $kH1$, porosity β, ratio of thickness of two layers ($D.R. = H2/H1$) and bonding parameter ψ are taken as 0.1, 0.3, 2 and 1.0 respectively, if not mentioned otherwise.

In this paper, the technique of transfer matrices has been used. The technique is popular and is widely reported for modelling wave propagation in layered structures. It is known fact that a transfer matrix is sometimes ill-conditioned and numerical instabilities occur especially when either the overall thickness of the layer or the frequency of the waves becomes very high, i.e., when the factor $kH1$ assumes larger values. These instabilities propagate during the subsequent computation and hence get amplified.

Various attempts have been made to reduce these instabilities. Dunkin [24] developed a delta operator technique which was improved by Kundu and Mal [25], Levesque and Piche [26] and Castings and Hosten [27]. Schmidt and Jensen [28] proposed a different approach whereby local equations for two layer sets are mapped into global system that comprises all unknowns associated with boundary conditions. In this case effectiveness depends on the stability of the Gaussian elimination technique used in the numerical computation. But for n layers, where n is large, the advantage of transfer matrix method is obvious because this method involves n-operation process while mapping technique is the n^2 or even n^3-operation process, depending upon the sparseness of the global system. Levesque and Piche [26] demonstrated, with the help of comparative studies that the transfer matrix technique provides a complete representation for the frequency, time and spatial dependence of the acoustic field.

Though the numerical calculations, in this study, were done for low frequency waves (small values of $kH1$), the numerical instability due to ill-conditioned matrix elements occur here also at some points. The numerical errors in ill-conditioned matrix are due to the presence of both growing and decaying terms in the elements of transfer matrix. As reported by Castings and Hosten [27], the closed form expressions for the local transfer matrix elements and sub determinants need to be found using mathematical software that perform symbolic operations. In our case, the transfer matrix was obtained in closed form expressions. The analytical expressions of all elements were arranged in such a way that higher order terms get multiplied with the lower

order terms which limit the order of terms to certain threshold at the lowest level in order to prevent instabilities due to precision inaccuracies. In fact, the modified expressions were obtained by grouping the terms when the matrices $[\Gamma_p]$ and $[\Gamma_p]^{-1}$ were multiplied. This controls the abrupt increase or decrease in the order of elements of transfer matrix and thus the local transfer matrix gets stabilized.

In Fig. 2a, the effect of porosity of TIPS layer on reflection coefficient is shown. The figure depicts the absolute value of the coefficient with varying angle of incidence for the porosity $\beta = 0.0001$, 0.1, 0.3 and 0.5 at $kH1 = 0.1$. It is observed that the reflection coefficient of P wave in FHS depends upon the porosity of the adjoining porous layer significantly. The effect of porosity is predominant before the critical angle (15°) for the transmitted quasi-P wave. In this range, the reflection coefficient increases with the porosity. When the porosity of the layer is very small, i.e., the layer is effectively a TIES layer, then the peaks of the reflection coefficient (solid curve) are not so sharp. This is probably due to the negligible effect of second kind of dilatational wave in the case. As the porosity increases, the first peak gets heightened showing the presence of second P

Table 2
Material constants for TIES layer, EHS and FHS

	TIES	TIEHS	FHS
Elastic constants (dyn/cm^2)	$A^{s(2)} = 75$ $C^{s(2)} = 50$ $F^{s(2)} = 17.092$ $L^{s(2)} = 11.42$	$A^{s(3)} = 90.26$ $C^{s(3)} = 83$ $F^{s(3)} = 48.65$ $L^{s(3)} = 14.9$	$\lambda = 2.2$
Density (g/cm^3)	$\rho^{s(2)} = 2.1$	$\rho^{s(3)} = 2.6$	$\rho = 1.0$

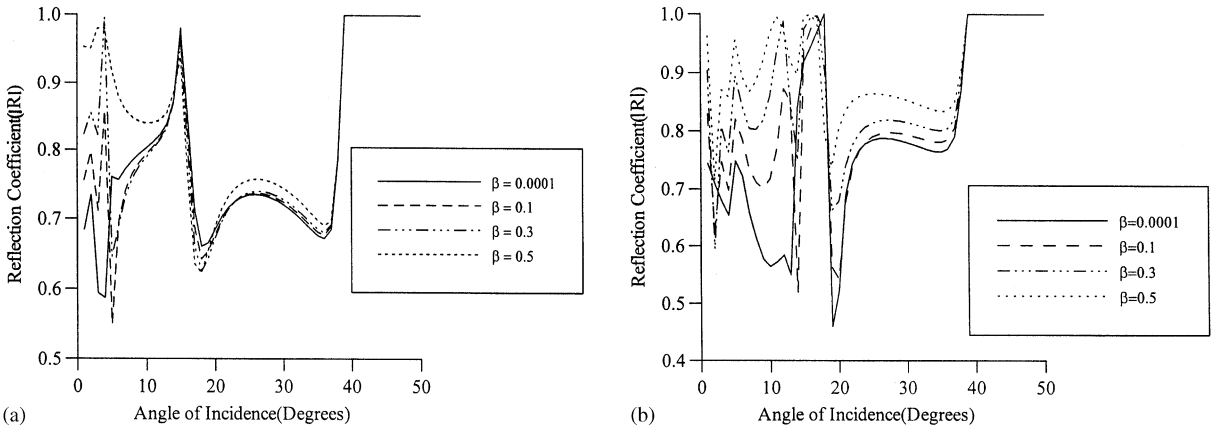

Fig. 2. Variation of reflection coefficient with angle of incidence for different values of porosity β at (a) $kH1 = 0.1$, (b) $kH1 = 0.3$.

wave. The amplitude of reflection coefficient corresponding to this peak increases as the porosity is increased.

In Fig. 2b, the variations of absolute value of the reflection coefficient is shown for different values of porosity at $kH1 = 0.3$. The effect of porosity is better observed in this case than that for lower value of $kH1$. The effect of porosity is also prominently felt for greater range of angle of incidence, while for lower value of $kH1$, this was only up to second critical angle. Moreover, as porosity increases, the magnitude of reflection coefficient also increases. The positions of critical angles are shifted towards right in this case. It is known that critical angles are those angles beyond which the P and S waves become the surface waves at the interface [29].

Fig. 3 shows the variation of reflection coefficient with angle of incidence at three different values of non-dimensional wave number $kH1 = 0.1$, 0.3, 0.5. The number of kinks in the reflection coefficient increases with the increase in $kH1$. This implies that for fixed $H1$, the number of kinks increases as the wavelength of the wave decreases. This observation is physically acceptable as the short wavelength waves are trapped in a layer.

To study the effect of the wave number $kH1$ on the reflection coefficient, $|R|$ was calculated at an incident angle of 10° for the different values of porosity and plots are shown in the Fig. 4. As observed in earlier graphs, the magnitude of reflection coefficient increases with the increase in porosity. The curve for $\beta = 0.1$ shows some different behavior from the other two curves for $\beta = 0.3$ and 0.5, in the starting range of $kH1$.

The effect of ratio of the thickness of TIES layer to the thickness of TIPS layer, $D.R.$, on the reflection coefficient is shown in Figs. 5a–c at different values of $kH1 = 0.1$, 0.5, 0.8. When $D.R. = 0$, then only TIPS layer is present in the model. Fig. 5a shows that there is a smooth variation in $|R|$ with the change in $D.R.$ The effect of TIES layer increases as the $D.R.$ increases. The change in reflection coefficient is noticeable corresponding to these changes in the thickness of layers. The sensitivity of the reflection coefficient is understood from the fact that the small changes in the thickness of TIPS layer can result in a relatively large change in the gradient of the velocity profile. By changing the thickness of TIPS layer, the wave-guide like nature of the sedimentary layer changes which, in turn, affects the velocity profile and hence the reflection phenomenon. However, the position of critical angles is not altered by the change in thickness at $kH1 = 0.1$. For higher values of $kH1$, the critical angles vary in number and position. Total

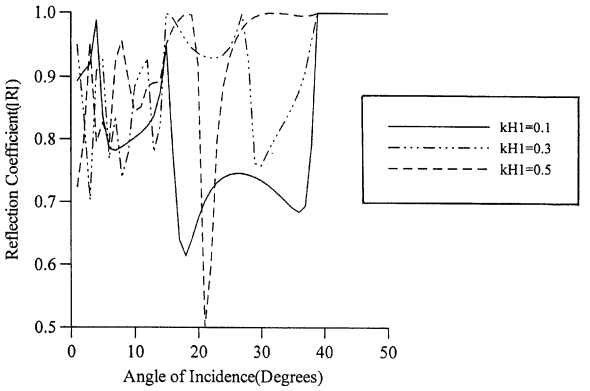

Fig. 3. Variation of reflection coefficient with angle of incidence for $kH1 = 0.1$, 0.3, 0.5.

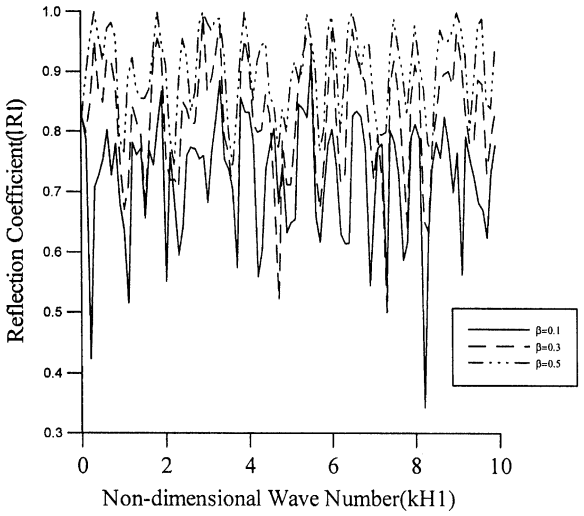

Fig. 4. Variation of reflection coefficient with non-dimensional wave number $kH1$ at angle of incidence 10°.

internal reflection, for the values $kH1 = 0.5$ and 0.8, occurs earlier in the comparison to $kH1 = 0.1$.

Fig. 6 shows the variation of reflection coefficient $|R|$ with frequency for two different values of thickness $H1$ of TIPS layer (i.e., $H1 = 100$ m and $H1 = 200$ m). The reflection coefficient shows the periodic behavior. It repeats itself in small frequency ranges.

One of the main objectives of the study is to observe the effect of anisotropy of medium on the reflection–transmission phenomena. $|R|$ was computed for the whole model to be transversely isotropic and for the case when both the layers and the half-space are isotropic. The comparison is shown in Fig. 7a. There is a qualitative change in the two curves before the incident angle 6° and after that both the curves are of same type. The difference between the two curves clearly indicates the necessity to incorporate the anisotropy in a mathematical model. Further, the effect of degree of anisotropy on reflection coefficient was also studied and the results are shown in the Fig. 7b. The results were computed for four different data sets ((a)–(d)) of values of the elastic coefficients. It is noticed from this figure that the reflection phenomenon is affected remarkably by the degree of anisotropy. One of the interesting points of observation is the advancement of the critical angle, for the transmitted quasi-P wave, towards left with the increase in the degree of anisotropy of the model. The other point of investigation is to find the layer whose degree of anisotropy influences the results the most. We allowed to vary the degree of anisotropy of each layer one by one and computed the values of $|R|$. It is observed that the results are the most affected by the increment in the degree of anisotropy of the half-space (see Fig. 7c) and the increase in the degree of anisotropy of porous layer does not change the reflection coefficient, significantly. To make the effect of anisotropy of each layer on the reflection coefficient clearer, the results were computed for the following cases:

(1) elastic layer and the half-space are transversely isotropic and the poro elastic layer is isotropic (Fig. 7d);

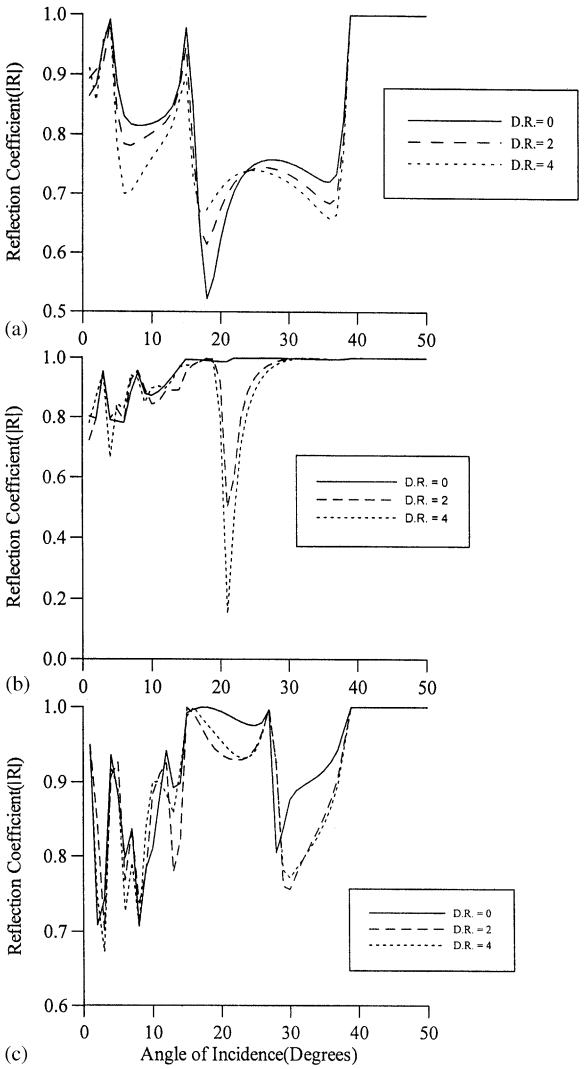

Fig. 5. Variation of reflection coefficient with angle of incidence for different values of ratio of thickness of layers at (a) $kH1 = 0.1$, (b) $kH1 = 0.5$, (c) $kH1 = 0.8$.

(2) poroelastic layer and the half-space are transversely isotropic and the elastic layer is isotropic (Fig. 7e);
(3) both the layers are isotropic and the half-space is transversely isotropic (Fig. 7f).

It is clear from the figures that the anisotropy of the porous layer is not affecting the results very much but the effect of anisotropy of the elastic layer and the half-space is noticeable. Fig. 7e shows the reflection coefficient when we model the elastic layer as isotropic one. The difference between the three curves in Figs. 7e and f emphatically depicts the fact that between the elastic layer and half-space, it is the half-space whose anisotropy dominates the results. In Fig. 7f, the effect of increase in the anisotropy of half-space is displayed. The position of critical angles is

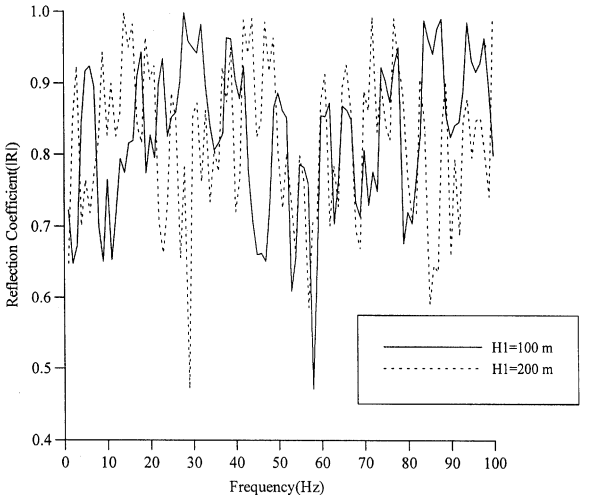

Fig. 6. Variation of reflection coefficient with frequency at angle of incidence 10°.

altered as the half-space is changed from isotropic one to strong anisotropic. Also, the behavior of reflection coefficient for strong anisotropic half-space, is different (one additional peak is visible in the curve). The minima are also moving towards left.

Figs. 8a–e illustrate the effects of imperfect bonding between the TIPS layer and TIES layer, on the reflection coefficient at different values of $kH1$ (i.e., $kH1 = 0.1$, 0.3, 0.5, 0.8, 1.0). The reflection curve at $kH1 = 0.1$ for different values of ψ (i.e., $\psi = 1.0$, 0.75, 0.50, 0.25) clearly depicts the effect of loose bonding (see Fig. 8a). The value of bounding parameter ψ is one in the case of welded contact between the porous layer and the elastic layer. The total internal reflection takes place nearly at incident angle 40° for welded contact. However, in case of loosely bonded interface, i.e., when $\psi = 0.75$, 0.5 and 0.25, the dissipation of energy is observed even after 40°. This behavior clearly matches with the established fact that loose boundaries are absorbing boundaries and energy is dissipated at such boundaries which results the decrease in magnitude of the reflection coefficient. The value of the non dimensional wave number is increased to 0.3 in the next step and Fig. 8b shows the results in this case. The dissipation of energy is more than that for $kH1 = 0.1$ and this increases further when the value of $kH1$ increases. This implies that when the thickness of the first layer is comparable to the wavelength of the wave, then the effects of loose boundary are significant. It is also observed that the bonding parameter affects the reflection coefficient prominently after 20°, for all the values of $kH1$. One interesting feature noted is that $|R|$ becomes unity at 45°, 49°, 55° and 61° for $kH1 = 0.3$, 0.5, 0.8 and 1.0, respectively (see Figs. 8b–e). These are the angles analogous to those in welded contact, at which total internal reflection takes place for respective values of $kH1$.

The effect of different layers of anisotropic substratum on reflection coefficient is exhibited in Fig. 9a. $|R|$ for different combinations of layers of the model is plotted. The results for the following particular models are computed and compared:

(a) when the complete model including both transversely isotropic layers, is considered;
(b) when the TIPS layer is not included in the model;

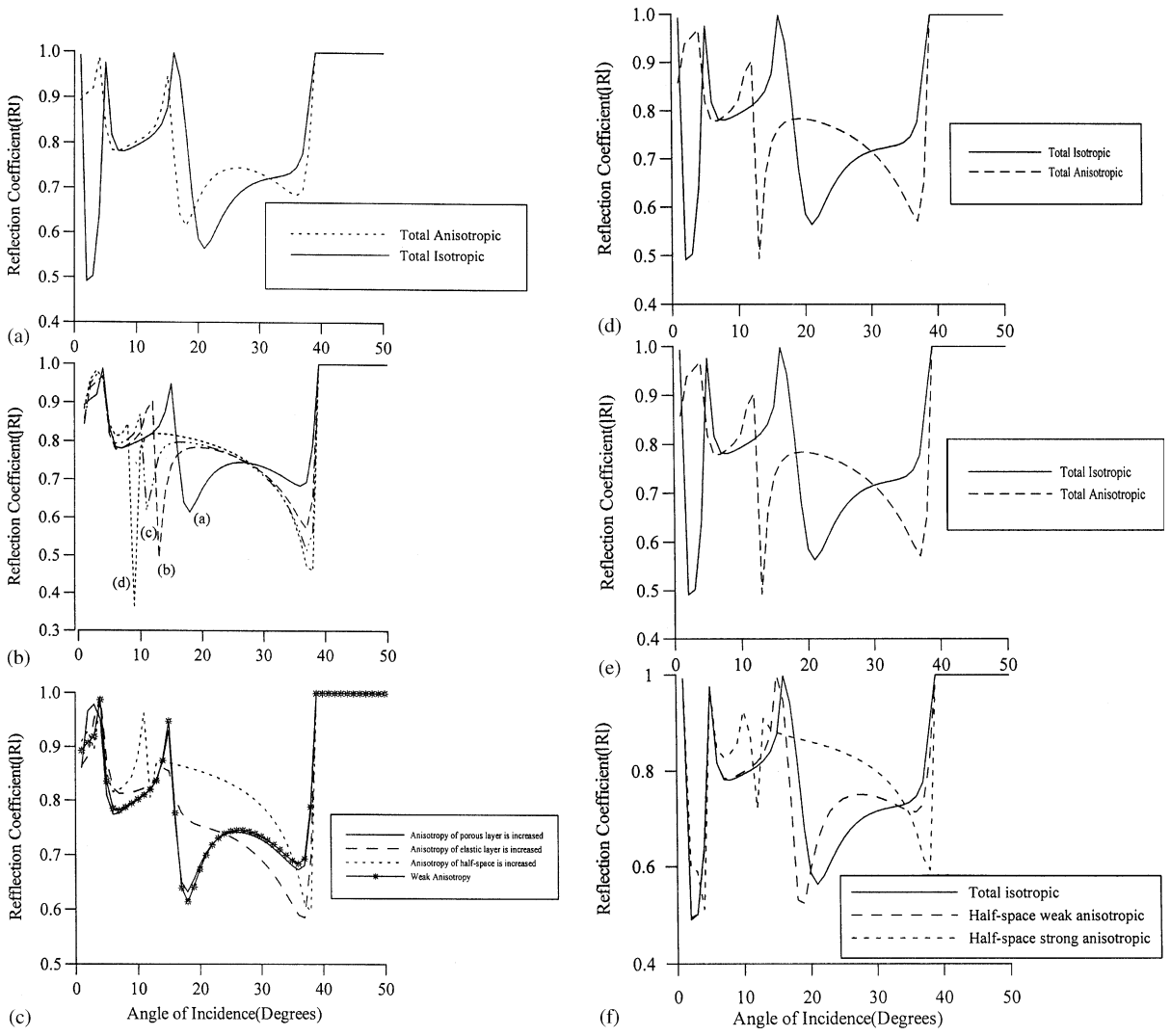

Fig. 7. Variation of reflection coefficient with angle of incidence for different degrees of anisotropy.

(c) when the TIES layer is not included in the model;
(d) when both the layers are not included in the model.

The results shown in the figure are computed for $kH1 = 0.3$ and $\beta = 0.5$. The effect of layers of different materials is clearly demonstrated.

An important feature of the study carried out is the generality of the model studied. All the models mentioned above, which find applications in seismology and engineering, are obtained as particular cases of the study. It is observed that the presence of the TIES layer in the model has a significant effect on the magnitude of the reflection coefficient. It attains its minimum value when elastic layer is not included in the model. Also, the magnitude decreases when either of the layers or both of the layers are absent.

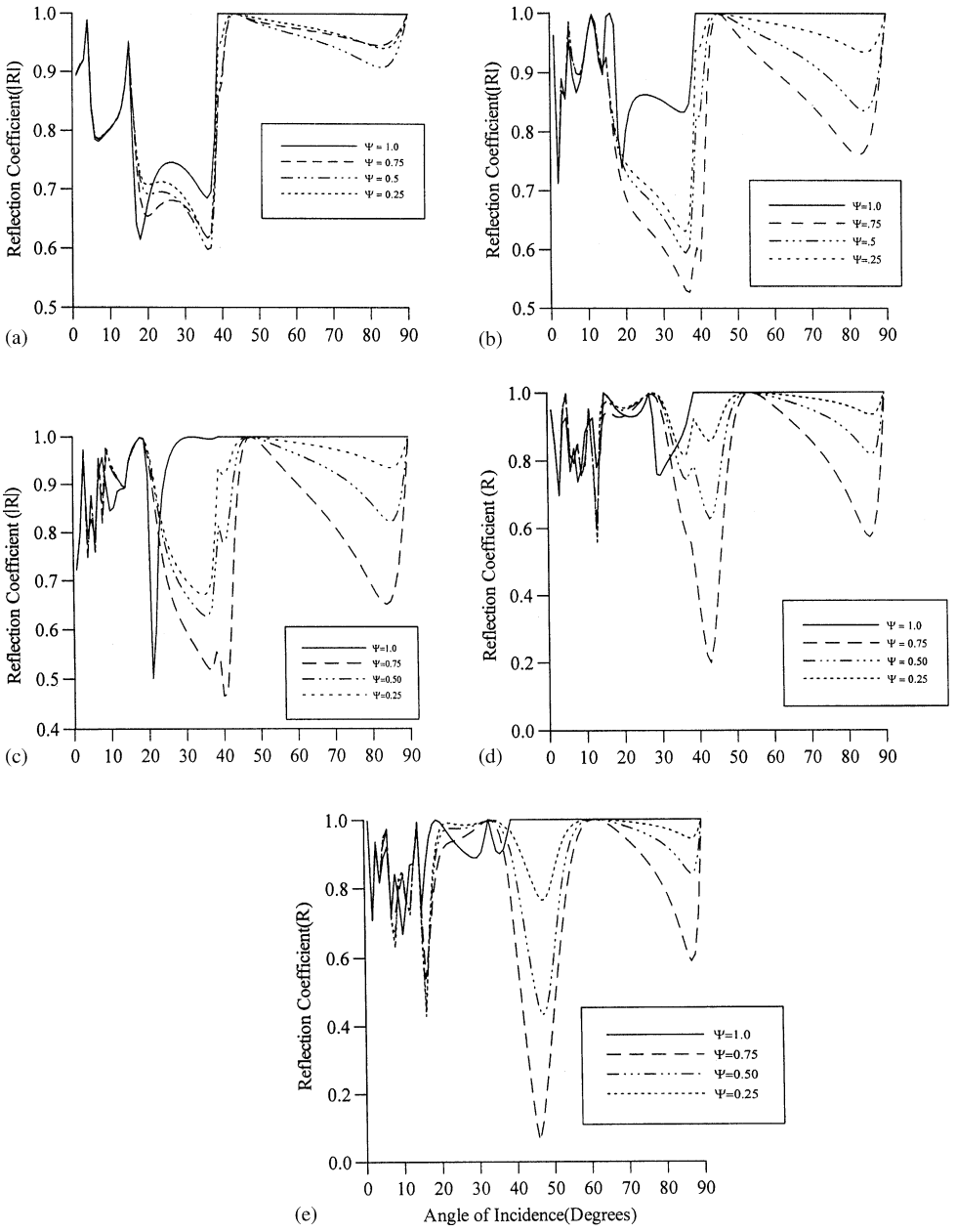

Fig. 8. Variation of reflection coefficient with angle of incidence for different values of ψ at (a) $kH1 = 0.1$, (b) $kH1 = 0.3$, (c) $kH1 = 0.5$, (d) $kH1 = 0.8$, (e) $kH1 = 1.0$.

To check the validity of the numerical model and the accuracy of the codes developed for computation, a well-known case of reflection and refraction at FHS–EHS interface is reduced from the considered model. The elastic half-space is considered isotropic one. The result is displayed in Fig. 9b. The result agrees with that mentioned in the text of Ewing et al. [29].

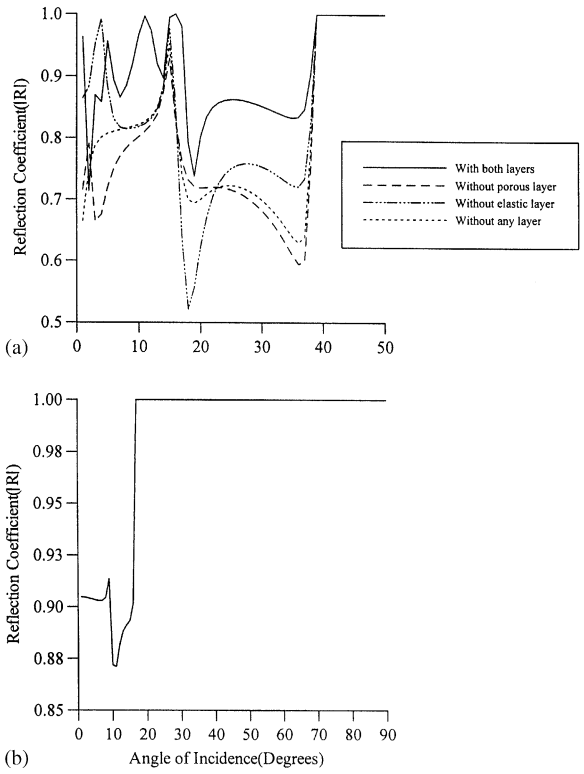

Fig. 9. (a) Variation of reflection coefficient with angle of incidence for different models at $kH1 = 0.3$ and porosity $\beta = 0.5$; (b) reflection coefficient at FHS–EHS interface.

Figs. 10a and b illustrate the variations in absolute values of transmission coefficients for quasi-P and SV waves, respectively, with angle of incidence for $kH1 = 0.1$ and for different values of porosity β. The effect of porosity on transmission of waves in TIES half-space is displayed in the figures. For lower values of incident angle (up to 15°), the effect of porosity is more counted than that at greater incident angle. The amplitude of the refracted quasi-SV wave increases sharply from 20° to 40° and the amplitude of refracted quasi-P wave decreases and tend to zero as incident wave approaches to normal incidence. In Figs. 11a and b, the effects of porosity on transmission coefficients are shown for $kH1 = 0.3$ and there is considerable difference between the transmission curves for $kH1 = 0.1$ and 0.3. For $kH1 = 0.3$, the amplitude of transmission coefficient of the quasi-P and SV waves are affected by the porosity of the first layer.

The effect of non dimensional wave number on transmission coefficients is shown in the Figs. 12a and b. The magnitudes of transmission coefficients were computed for different values of $kH1 = 0.1$, 0.3, 0.5, 0.8. The non-dimensional wave number, considerably, affects the transmission of the waves. As the value of $kH1$ increases from 0.1 to 0.8, number of peaks increases. Also, the increment in $kH1$ increases the amplitude of the transmission coefficients.

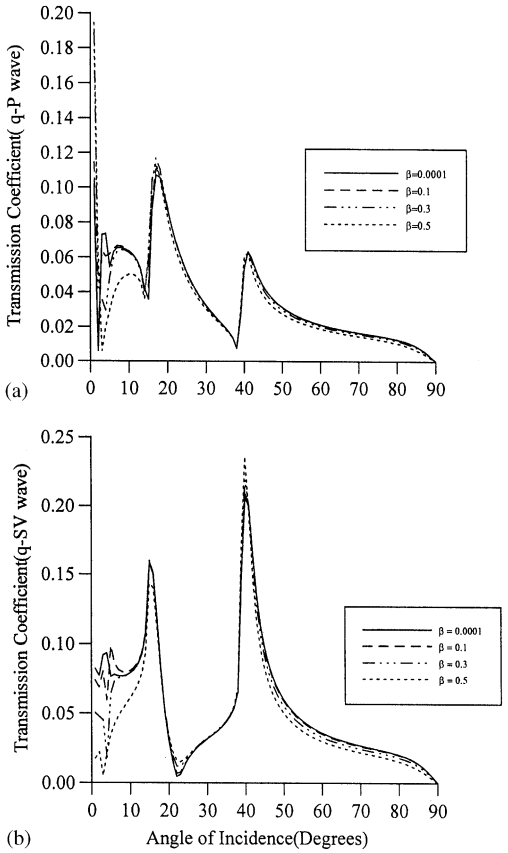

Fig. 10. Variation of transmission coefficient with angle of incidence at $kH1 = 0.1$ for (a) q-P wave, (b) q-SV wave.

Figs. 13a and b display the effect of loose bonding, between the layers, on transmission coefficients of quasi-P and SV waves, respectively, at $kH1 = 0.1$. At this value of $kH1$, the effect is not so clear. A little decrease in the amplitude is observed at $kH1 = 0.1$ due to the loose bonding. But, for $kH1 = 0.3$, a significant effect of loose bonding on transmission coefficients is observed and the graphs show this in the Figs. 14a and b. Both the transmission coefficients are behaving differently towards loose bonding. Amplitude of transmitted quasi-P wave increases with imperfection of the interface in the range 12–38° and, then after 46°, it again increases. In the case of quasi-SV wave, there is a considerable difference between its peak magnitudes for welded contact and loose boundary.

Figs. 15a and b exhibit the effect of anisotropy of the model on transmission coefficients of quasi-P and SV waves. It is noted that the transmission coefficients of quasi-P and SV waves show the same type of behavior between the range 20° and 40° in isotropic model while the transmission coefficient are of opposite nature, in this range, in case of transversely isotropic model. Anisotropy of the medium causes difference between them. The amplitude of transmission coefficient of quasi-P wave increases due to the anisotropy of complete model in the range of 5–17°. The transmission coefficient of quasi-SV wave shows this behavior in little earlier range of

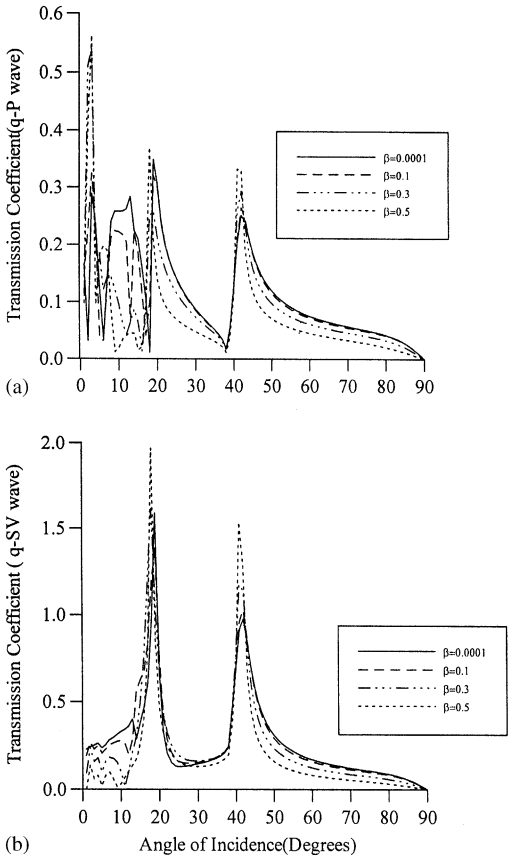

Fig. 11. Variation of transmission coefficient with angle of incidence at $kH1 = 0.3$ for (a) q-P wave, (b) q-SV wave.

angle of incidence. It is the matter of further investigation that the anisotropic half-space alone affects the transmission coefficients. To study this, the transmission coefficients of quasi-P and -SV waves are plotted for the model when only EHS is transversely isotropic and the other two layers are isotropic. The comparison of the curves in Figs. 15a and b implies that the anisotropy of the half-space affect the transmission up to a great extent and at the same time, the anisotropy of both the layers is equally important.

In Fig. 16a, the real and imaginary part of the reflection coefficients R are plotted against the angle of incidence. The real part of the reflection coefficient attains its minimum value (i.e., -1) at the incident angle 39°. The imaginary part also suffers a sharp change near this angle. This angle coincides with the one after which total internal reflection takes place. The recognition of the minimum of real part of R at such an angle gives a criterion of identification of surface wave modes [7].

To plot the dispersion curves of surface waves propagating in the considered model, the angle where the minima of Re(R) occurs for different values of $kH1$, are identified. Using Snell's law, the phase velocity, corresponding to these angles, as a function of $kH1$ is evaluated. The

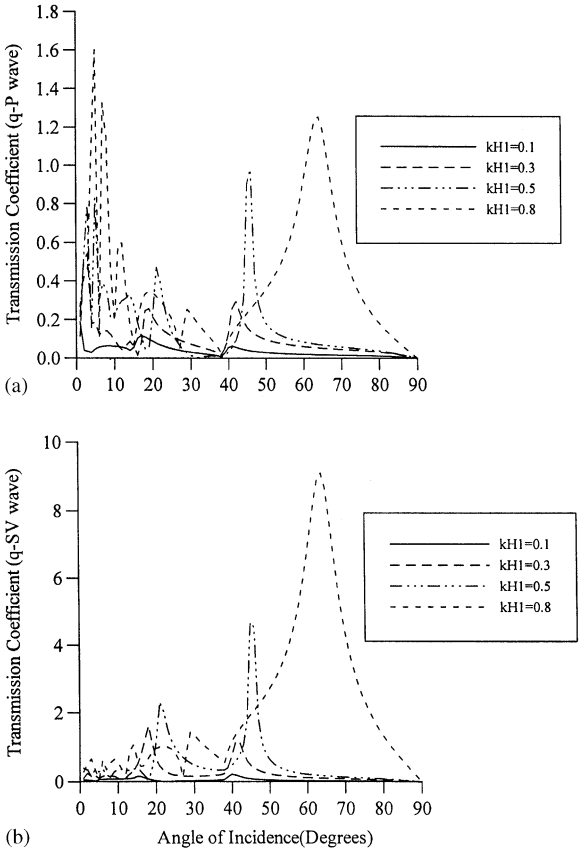

Fig. 12. Variation of transmission coefficient with angle of incidence for different values of $kH1$ for (a) q-P wave, (b) q-SV wave.

dispersion curves of surface waves, so obtained, are shown in Fig. 16b, for two different values of porosity β. Only fundamental modes are shown in the figure. The phase velocity of the surface waves increases with the increment in porosity of the first layer.

To justify the fact that the roots of Eq. (10), a cubic in q^2, are non-repeated, the wave velocities of the quasi-P_f, quasi-P_s and quasi-SV waves were computed using the three roots of Eq. (10) and these are shown in Fig. 17 as a function of the angle between the direction of propagation of wave and the z-axis. As established, the wave velocities depend on the direction of propagation in a transversely isotropic medium.

In Fig. 18, comparison between reflection coefficients of reflected P wave for the three models is made. These models refer to

(i) Model R1 Dorman et al. [30]
(ii) Model 94 Phinney and Alexander [31]
(iii) Model 81 Phinney and Alexander [31]

and the associated data is given in Table 3.

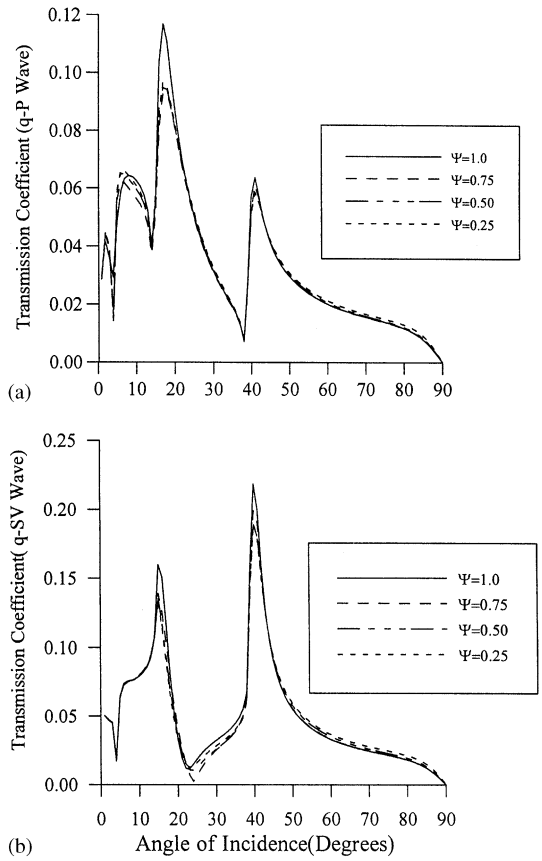

Fig. 13. Variation of transmission coefficient with angle of incidence at $kH1 = 0.1$ for different values of ψ for (a) q-P wave, (b) q-SV wave.

The three curves are obtained at incident angle of 60° for the period 0–100 s. This reflection coefficient is associated with the seismic PcP phase. The curves obtained in the present study match with the ones obtained by Teng [32]. The amplitudes for the model 2 and model 3 are distinct from the model 1. As studied by Teng [32], the PcP shows the sensitivity to the core–mantle boundary structure.

10. Conclusion

Wave propagation in a multilayered medium is studied in detail. The analysis of the problem is done by using the transfer matrices. The reflection and transmission coefficients are obtained in terms of global matrix elements. Numerical computations are done for a particular model which consists of TIPS and TIES layers overlying a TIES half-space and underlying FHS. The effects of various parameters e.g., anisotropy, porosity, non-dimensional wave number, frequency, imperfect bonding between the layers on reflection–transmission phenomenon are studied.

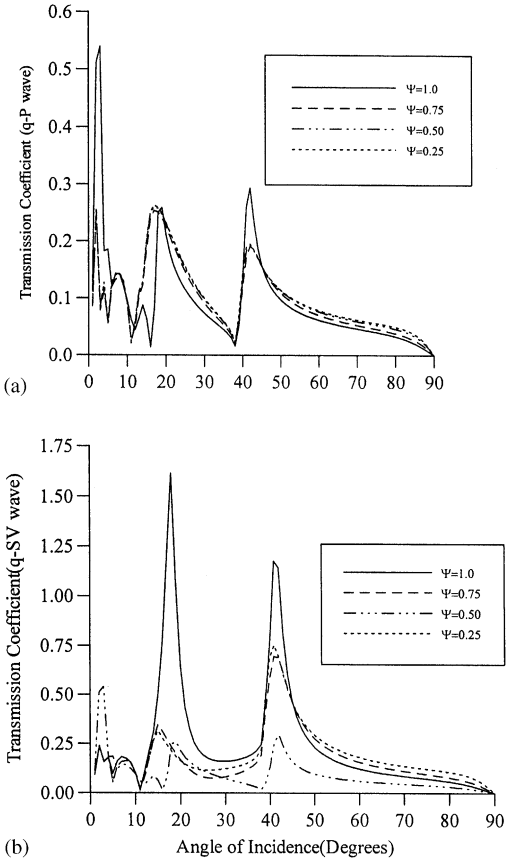

Fig. 14. Variation of transmission coefficient with angle of incidence at $kH1 = 0.3$ for different values of ψ for (a) q-P wave, (b) q-SV wave.

It is observed that the increment in porosity increases the magnitude of the reflection coefficient. The main purpose of this study is the investigation of the effect of anisotropy on the reflection and transmission of waves through a layered medium. The phenomenon is influenced significantly by the anisotropy of the medium and it is the anisotropy of half-space which is influencing the most. This may be the point of further investigation. Also, it is noticed that the loose bonding between the layers is accompanied by the dissipation of energy and hence decreases the reflection and transmission of energy.

The characteristic equations for the surface waves propagating along the fluid-loaded anisotropic layered substrate and for the free surface waves propagating along the anisotropic layered substrate are obtained. The phase velocity curves for the surface waves propagating along the fluid-loaded anisotropic layered substrate are plotted by recording the minima in the reflection coefficient. The effect of porosity on the phase velocity is observed.

The study is of practical interest because of the current importance attached to the use of composite materials in wide variety of applications. Typically, the composite structural

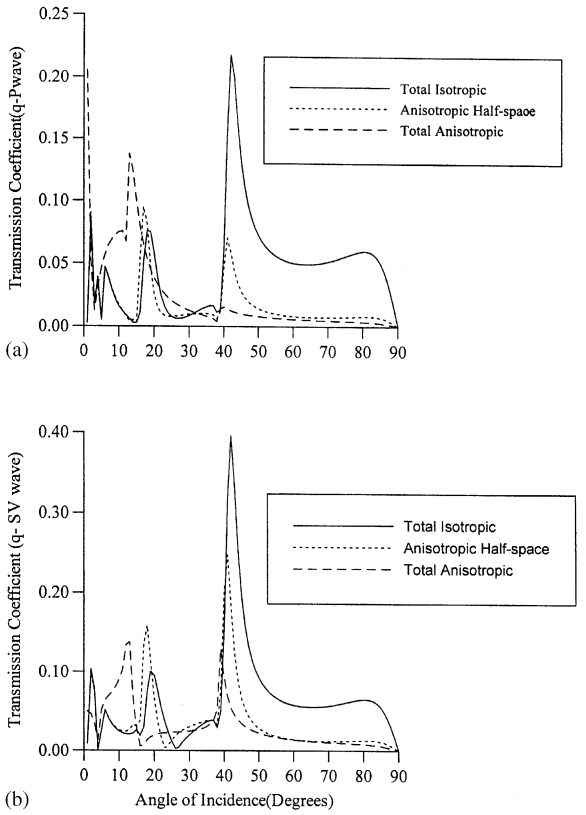

Fig. 15. Variation of transmission coefficient with angle of incidence for (a) q-P wave, (b) q-SV wave.

components are made up of stack of layers. The modelling of wave propagation in layered anisotropic media may also find its application in seismology.

Acknowledgements

The first author is thankful to the Department of Science and Technology, Government of India for supporting the work. The authors are thankful to reviewers for their critical analysis and valuable comments.

Appendix A

$$\gamma_{11}^{(p)} = \frac{\cos(\omega q^{(p)}(1)z)}{M^{(p)}}, \quad \gamma_{12}^{(p)} = \frac{\mathrm{i}\sin(\omega q^{(p)}(1)z)}{N^{(p)}}, \quad \gamma_{13}^{(p)} = -\frac{\mathrm{i}\sin(\omega q^{(p)}(1)z)}{N^{(p)}} Q_1^{(p)},$$

$$\gamma_{14}^{(p)} = -\frac{\cos(\omega q^{(p)}(1)z)}{M^{(p)}} R_1^{(p)}, \quad \gamma_{15}^{(p)} = -\frac{\mathrm{i}\sin(\omega q^{(p)}(1)z)}{N^{(p)}} S_1^{(p)}, \quad \gamma_{16}^{(p)} = -\frac{\cos(\omega q^{(p)}(1)z)}{M^{(p)}} L_1^{(p)},$$

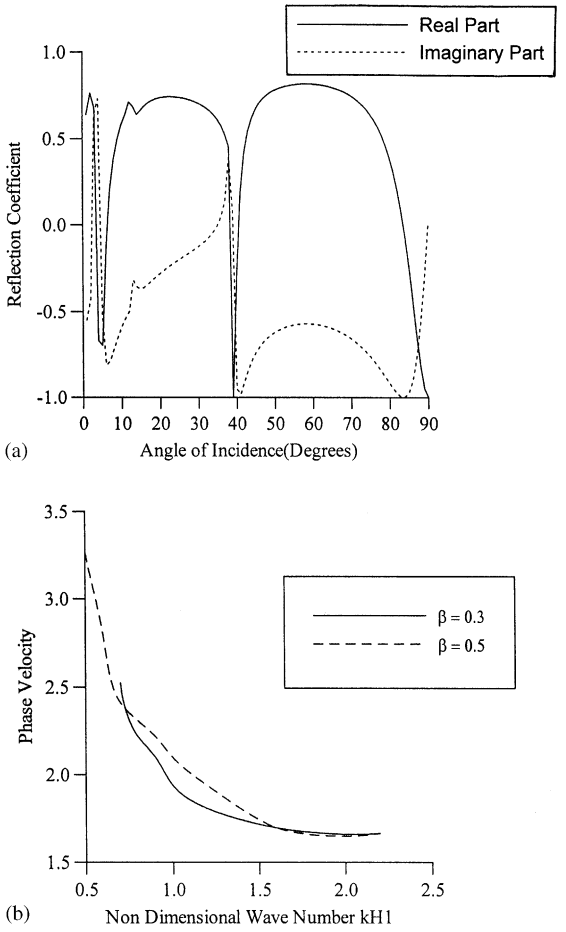

Fig. 16. (a) Variation of real and imaginary parts of reflection coefficient with angle of incidence; (b) variation of phase velocity with non-dimensional wave number.

$$\gamma_{21}^{(p)} = \frac{\mathrm{i}\sin(\omega q^{(p)}(1)z)}{M^{(p)}}, \quad \gamma_{22}^{(p)} = \frac{\cos(\omega q^{(p)}(1)z)}{N^{(p)}}, \quad \gamma_{23}^{(p)} = -\frac{\cos(\omega q^{(p)}(1)z)}{N^{(p)}} Q_1^{(p)},$$

$$\gamma_{24}^{(p)} = -\frac{\mathrm{i}\sin(\omega q^{(p)}(1)z)}{M^{(p)}} R_1^{(p)}, \quad \gamma_{25}^{(p)} = -\frac{\cos(\omega q^{(p)}(1)z)}{N^{(p)}} S_1^{(p)}, \quad \gamma_{26}^{(p)} = -\frac{\mathrm{i}\sin(\omega q^{(p)}(1)z)}{N^{(p)}} L_1^{(p)},$$

$$\gamma_{31}^{(p)} = -H^{(p)}\frac{\cos(\omega q^{(p)}(2)z)}{M^{(p)}}, \quad \gamma_{32}^{(p)} = -G^{(p)}\frac{\mathrm{i}\sin(\omega q^{(p)}(2)z)}{N^{(p)}}, \quad \gamma_{33}^{(p)} = \mathrm{i}\sin(\omega q^{(p)}(2)z)Q_2^{(p)},$$

$$\gamma_{34}^{(p)} = -\cos(\omega q^{(p)}(2)z)R_2^{(p)}, \quad \gamma_{35}^{(p)} = \mathrm{i}\sin(\omega q^{(p)}(2)z)S_2^{(p)}, \quad \gamma_{36}^{(p)} = \cos(\omega q^{(p)}(2)z)L_2^{(p)},$$

$$\gamma_{41}^{(p)} = -H^{(p)}\frac{\mathrm{i}\sin(\omega q^{(p)}(2)z)}{M^{(p)}}, \quad \gamma_{42}^{(p)} = -\frac{\cos(\omega q^{(p)}(2)z)}{N^{(p)}} G^{(p)}, \quad \gamma_{43}^{(p)} = \cos(\omega q^{(p)}(2)z)Q_2^{(p)},$$

$$\gamma_{44}^{(p)} = -\mathrm{i}\sin(\omega q^{(p)}(2)z)R_2^{(p)}, \quad \gamma_{45}^{(p)} = \cos(\omega q^{(p)}(2)z)S_2^{(p)}, \quad \gamma_{46}^{(p)} = \mathrm{i}\sin(\omega q^{(p)}(2)z)L_2^{(p)},$$

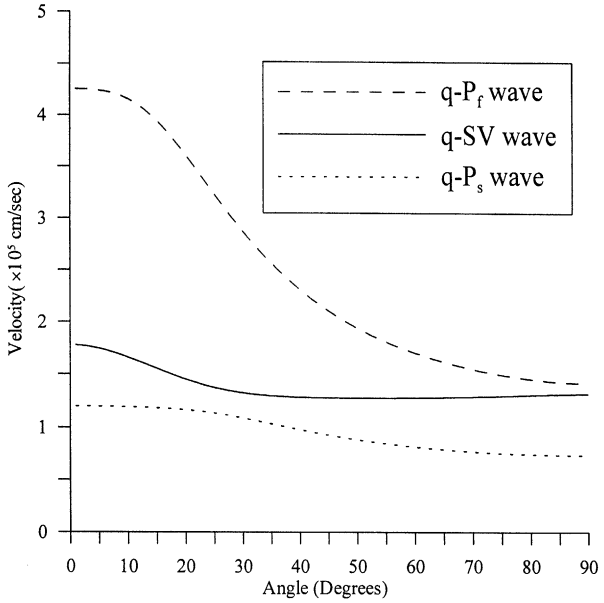

Fig. 17. Wave velocity as a function of direction of propagation.

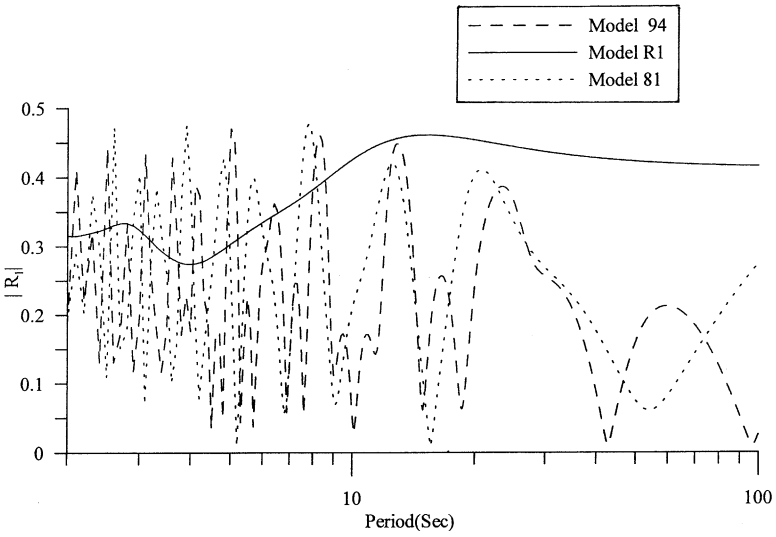

Fig. 18. Reflection coefficient of reflected P-wave due to P-wave incident in the mantle against core.

Table 3
Models of core–mantle boundary

Model no.	Layer no.	Thickness (km)	α (km/s)	β (km/s)	ρ (g/cm^3)
1	0	∞	8.150	0.000	9.400
	1	11.00	10.200	5.200	6.200
	2	13.00	11.600	6.100	5.670
	3	12.00	13.000	6.840	5.660
	4	∞	13.690	7.210	5.650
2	0	∞	8.300	0.000	9.500
	1	30	10.000	2.800	6.700
	2	∞	13.600	7.500	5.500
3	0	∞	8.300	0.00	9.500
	1	100	13.30	4.800	6.700
	2	∞	13.60	7.500	5.500

$$\gamma_{51}^{(p)} = H^{*(p)}\frac{\cos(\omega q^{(p)}(3)z)}{M^{(p)}}, \quad \gamma_{52}^{(p)} = G^{*(p)}\frac{\mathrm{i}\sin(\omega q^{(p)}(3)z)}{N^{(p)}}, \quad \gamma_{53}^{(p)} = -\mathrm{i}\sin(\omega q^{(p)}(3)z)Q_3^{(p)},$$
$$\gamma_{54}^{(p)} = \cos(\omega q^{(p)}(3)z)R_3^{(p)}, \quad \gamma_{55}^{(p)} = -\mathrm{i}\sin(\omega q^{(p)}(3)z)S_3^{(p)}, \quad \gamma_{56}^{(p)} = -\cos(\omega q^{(p)}(3)z)L_3^{(p)},$$
$$\gamma_{61}^{(p)}\frac{\mathrm{i}\sin(\omega q^{(p)}(3)z)}{M^{(p)}}H^{*(p)}, \quad \gamma_{62}^{(p)} = \frac{\cos(\omega q^{(p)}(3)z)}{N^{(p)}}G^{*(p)}, \quad \gamma_{63}^{(p)} = -\cos(\omega q^{(p)}(3)z)Q_3^{(p)},$$
$$\gamma_{64}^{(p)} = \mathrm{i}\sin(\omega q^{(p)}(3)z)R_3^{(p)}, \quad \gamma_{65}^{(p)} = -\cos(\omega q^{(p)}(3)z)S_3^{(p)}, \quad \gamma_{66}^{(p)} = -\mathrm{i}\sin(\omega q^{(p)}(3)z)L_3^{(p)},$$

where

$$X^{(p)} = \frac{D_3^{(p)}b_3^{(p)}(2) - D_2^{(p)}b_3^{(p)}(3)}{D_3^{(p)}}, \quad Y^{(p)} = \frac{C_2^{(p)}P_3^{(p)} - C_3^{(p)}P_2^{(p)}}{P_3^{(p)}},$$
$$M^{(p)} = a_1^{(p)}(1) + C_1^{(p)}R_1^{(p)} + P_1^{(p)}L_1^{(p)}, \quad N^{(p)} = a_3^{(p)}(1) - b_3^{(p)}(1)Q_1^{(p)} + D_1^{(p)}S_1^{(p)},$$
$$Q_1^{(p)} = \frac{D_3^{(p)}a_3^{(p)}(2) - D_2^{(p)}a_3^{(p)}(3)}{X^{(p)}D_3^{(p)}}, \quad Q_2^{(p)} = \left[\frac{1}{X^{(p)}} + G^{(p)}\frac{Q_1^{(p)}}{N^{(p)}}\right],$$
$$Q_3^{(p)} = \frac{D_2^{(p)}}{X^{(p)}D_3^{(p)}} + G^{*(p)}\frac{Q_1^{(p)}}{N^{(p)}}, \quad G^{(p)} = \frac{D_3^{(p)}b_3^{(p)}(1) - D_1^{(p)}b_3^{(p)}(3)}{X^{(p)}D_3^{(p)}},$$
$$G^{*(p)} = \frac{D_2^{(p)}b_3^{(p)}(1) - D_1^{(p)}b_3^{(p)}(2)}{X^{(p)}D_3^{(p)}}, \quad H^{(p)} = \frac{P_3^{(p)}C_1^{(p)} - C_3^{(p)}P_1^{(p)}}{Y^{(p)}P_3^{(p)}},$$
$$H^{*(p)} = \frac{P_2^{(p)}C_1^{(p)} - C_2^{(p)}P_1^{(p)}}{Y^{(p)}P_3^{(p)}}, \quad S_1^{(p)} = \frac{a_3^{(p)}(2)b_3^{(p)}(3) - a_3^{(p)}(3)b_3^{(p)}(2)}{X^{(p)}D_3^{(p)}},$$

$$S_2^{(p)} = \left[\frac{b_3^{(p)}(3)}{X^{(p)}D_3^{(p)}} + G^{(p)}\frac{S_1^{(p)}}{N^{(p)}}\right], \quad S_3^{(p)} = \left[\frac{b_3^{(p)}(2)}{X^{(p)}D_3^{(p)}} + G^{*(p)}\frac{S_1^{(p)}}{N^{(p)}}\right],$$

$$L_1^{(p)} = \frac{a_1^{(p)}(2)C_3^{(p)} - a_1^{(p)}(3)C_2^{(p)}}{Y^{(p)}P_3^{(p)}}, \quad L_2^{(p)} = \left[\frac{C_3^{(p)}}{YP_3^{(p)}} + H^{(p)}\frac{L_1^{(p)}}{M^{(p)}}\right],$$

$$L_3^{(p)} = \left[\frac{C_2^{(p)}}{YP_3^{(p)}} + H^{*(p)}\frac{L_1^{(p)}}{M^{(p)}}\right], \quad R_1^{(p)} = \frac{a_1^{(p)}(3)P_2^{(p)} - a_1^{(p)}(2)P_3^{(p)}}{Y^{(p)}P_3^{(p)}},$$

$$R_2^{(p)} = \left[\frac{1}{Y^{(p)}} - H^{(p)}\frac{R_1^{(p)}}{M^{(p)}}\right], \quad R_3^{(p)} = \left[\frac{P_2^{(p)}}{Y^{(p)}P_3^{(p)}} - H^{*(p)}\frac{R_1^{(p)}}{M^{(p)}}\right].$$

Appendix B

$$\Gamma_{11}^{s(q)} = \cos\theta_1^{(q)}, \quad \Gamma_{12}^{s(q)} = -\mathrm{i}\sin\theta_1^{(q)}, \quad \Gamma_{13}^{s(q)} = \cos\theta_2^{(q)},$$
$$\Gamma_{14}^{s(q)} = -\mathrm{i}\sin\theta_2^{(q)}, \quad \Gamma_{21}^{s(q)} = -m_1^{(q)}\mathrm{i}\sin\theta_1^{(q)}, \quad \Gamma_{22}^{s(q)} = m_1^{(q)}\cos\theta_1^{(q)},$$
$$\Gamma_{23}^{s(q)} = -m_2^{(q)}\mathrm{i}\sin\theta_2^{(q)}, \quad \Gamma_{24}^{s(q)} = m_2^{(q)}\cos\theta_2^{(q)}, \quad \Gamma_{31}^{s(q)} = X_1^{(q)}\mathrm{i}\cos\theta_1^{(q)},$$
$$\Gamma_{32}^{s(q)} = X_1^{(q)}\sin\theta_1^{(q)}, \quad \Gamma_{33}^{s(q)} = X_2^{(q)}\mathrm{i}\cos\theta_2^{(q)}, \quad \Gamma_{34}^{s(q)} = X_2^{(q)}\sin\theta_2^{(q)},$$
$$\Gamma_{41}^{s(q)} = Y_1^{(q)}\sin\theta_1^{(q)}, \quad \Gamma_{42}^{s(q)} = Y_1^{(q)}\mathrm{i}\cos\theta_1^{(q)}, \quad \Gamma_{43}^{s(q)} = Y_2^{(q)}\sin\theta_2^{(q)},$$
$$\Gamma_{44}^{s(q)} = Y_2^{(q)}\mathrm{i}\cos\theta_2^{(q)},$$

where

$$X_j^{(q)} = -k(C^{s(q)}s_j^{(q)}m_j^{(q)} + F^{s(q)}), \quad Y_j^{(q)} = -kL^{s(q)}(s_j^{(q)} + m_j^{(q)})$$

and

$$\theta_j^{(q)} = ks_j^{(q)}z \quad (j = 1, 2)$$
$$[\varepsilon^{(n+m+1)}] = [\varepsilon_{ij}^{(n+m+1)}],$$

where

$$\varepsilon_{11}^{(n+m+1)} = \mathrm{e}^{-\mathrm{i}ks_1^{(n+m+1)}z}, \quad \varepsilon_{12}^{(n+m+1)} = \mathrm{e}^{-\mathrm{i}ks_2^{(n+m+1)}z},$$
$$\varepsilon_{21}^{(n+m+1)} = m_1^{(n+m+1)}\mathrm{e}^{-\mathrm{i}ks_1^{(n+m+1)}z}, \quad \varepsilon_{22}^{(n+m+1)} = m_2^{(n+m+1)}\mathrm{e}^{-\mathrm{i}ks_2^{(n+m+1)}z},$$
$$\varepsilon_{31}^{(n+m+1)} = \mathrm{i}X_1^{(n+m+1)}\mathrm{e}^{-\mathrm{i}ks_1^{(n+m+1)}z}, \quad \varepsilon_{32}^{(n+m+1)} = \mathrm{i}X_2^{(n+m+1)}\mathrm{e}^{-\mathrm{i}ks_2^{(n+m+1)}z},$$
$$\varepsilon_{41}^{(n+m+1)} = \mathrm{i}\,Y_1^{(n+m+1)}\mathrm{e}^{-\mathrm{i}ks_1^{(n+m+1)}z}, \quad \varepsilon_{42}^{(n+m+1)} = \mathrm{i}\,Y_2^{(n+m+1)}\mathrm{e}^{-\mathrm{i}ks_2^{(n+m+1)}z}.$$

References

[1] M.A. Biot, Theory of propagation of elastic waves in a fluid-saturated porous solid—I: low frequency range, *Journal of the Acoustical Society of America* 28 (1956) 168–178.
[2] M.A. Biot, Theory of propagation of elastic waves in a fluid saturated porous solid—II: high frequency range, *Journal of the Acoustical Society of America* 28 (1956) 179–191.
[3] L.M. Brekhovskikh, *Waves in Layered Media*, Academic Press, New York, 1960.
[4] B.L. Kennet, *Seismic Wave Propagation in Stratified Media*, Cambridge University Press, New York, 1983.
[5] G.D. Briggs, *Acoustic Microscopy*, Clarendon Press, Oxford Science Publications, Oxford, 1992.
[6] G.S. Kino, *Acoustic Wave: Devices, Imaging, and Analog Signal Processing*, Prentice-Hall, N.S. Englewood Cliffs, NJ, 1987.
[7] A.H. Nayfeh, *Wave Propagation in Layered Anisotropic Media*, Elsevier Science, Amsterdam, 1995.
[8] A.H. Nayfeh, The general problem of elastic wave propagation in multilayered anisotropic media, *Journal of the Acoustical Society of America* 89 (4) (1991) 1521–1531.
[9] A.H. Nayfeh, D.E. Chimenti, Ultrasonic leaky waves in a solid plate separating a fluid and vacuum, *Journal of the Acoustical Society of America* 85 (1989) 555–560.
[10] K.P. Soldatos, J.Q. Ye, Wave propagation in anisotropic laminated hollow cylinders of infinite extent, *Journal of the Acoustical Society of America* 96 (5) (1994) 3744–3752.
[11] J.F. Allard, P. Bourdier, C. Depollier, Biot waves in layered media, *Journal of Applied Physics* 60 (1986) 1926–1929.
[12] J.F. Allard, R. Rebillard, C. Depollier, W. Lauriks, A. Cops, Inhomogeneous Biot waves in layered media, *Journal of Applied Physics* 66 (1989) 2278–2284.
[13] M. Badiey, L. Jaya, A.H.-D. Cheng, Propagator matrix for plane wave reflection from inhomogeneous anisotropic poroelastic seafloor, *Journal of Computational Acoustics* 2 (1994) 11–27.
[14] W. Lauriks, J.F. Allard, C. Depollier, A. Cops, Inhomogeneous waves in layered materials including fluid, solid and porous layers, *Wave Motion* 13 (1991) 329–336.
[15] C. Potel, Jean F. de Belleval, Propagation in an anisotropic periodically multilayered medium, *Journal of the Acoustical Society of America* 93 (5) (1993) 2669–2677.
[16] D.P. Schmitt, Acoustic multiple logging transversely isotropic poroelastic formations, *Journal of the Acoustical Society of America* 86 (6) (1989) 2398–2421.
[17] M.D. Sharma, M.L. Gogna, Wave propagation in anisotropic liquid-saturated porous solid, *Journal of the Acoustical Society of America* 90 (1991) 1068–1073.
[18] M.A. Biot, Mechanics of deformation and acoustic propagation in porous media, *Journal of Applied Physics* 33 (1962) 1482–1498.
[19] Z. Hashin, B.W. Rosen, The elastic moduli and fiber reinforced materials, *Journal of Applied Mechanics* 31 (1964) 223–232.
[20] R.M. Christensen, *Mechanics of Composite Materials*, Wiley, New York, 1979.
[21] A.E.H. Love, *A Treatise on Mathematical Theory of Elasticity*, 2nd Edition, Dover, New York, 1944.
[22] A.K. Vashishth, M.D. Sharma, M.L. Gogna, Reflection and transmission of elastic waves at a loosely bonded interface between an elastic solid and liquid saturated porous solid, *Geophysical Journal International* 105 (1991) 601–617.
[23] T. Yammamato, Acoustic propagation in the ocean with a poro elastic bottom, *Journal of the Acoustical Society of America* 83 (1983) 1587–1596.
[24] J.W. Dunkin, Computation of modal solutions in layered elastic media at high frequencies, *Bulletin of the Seismological Society of America* 55 (1965) 335–358.
[25] T. Kundu, A.K. Mal, Elastic waves in a multilayered solid due to a dislocation source, *Wave Motion* 7 (1985) 459–471.
[26] D. Levesque, L. Piche, A robust transfer matrix formulation for the ultrasonic response of multilayered absorbing media, *Journal of the Acoustical Society of America* 92 (1) (1992) 452–466.
[27] M. Castings, B. Hosten, Delta operator technique to improve the Thomson–Haskell-method stability for propagation in multilayered anisotropic absorbing plates, *Journal of the Acoustical Society of America* 95 (1994) 1931–1941.

[28] H. Schmidt, F.B. Jensen, A full wave solution for propagation in multilayered viscoelastic media with application to Gaussian beam reflection at solid–fluid interfaces, *Journal of the Acoustical Society of America* 77 (1985) 813–825.
[29] W.M. Ewing, W.S. Jardetsky, F. Press, *Elastic Waves in Layered Media*, McGraw-Hill, New York, 1957.
[30] J. Dorman, J. Ewing, L.E. Alsop, Oscillations of the earth: new core–mantle boundary model based on low order free vibrations, *Proceedings of the National Academy of Sciences* 54 (1965) 364–368.
[31] R.A. Phinney, S.S. Alexander, Diffraction of P waves and the structure of the core–mantle boundary, *Journal of Geophysical Research* 71 (1966) 5959–5975.
[32] Ta-Liang Teng, Reflection and transmission from a plane layered core–mantle boundary, *Bulletin of the Seismological Society of America* 57 (3) (1967) 477–499.